EXPERIMENTS ON PARITY NON-CONSERVATION IN NUCLEAR FORCES IN ^{180}Hf, ^{159}Tb, ^{203}Tl AND ^{181}Ta

Thesis by

Edward David Lipson

In Partial Fulfillment of the Requirements

for the Degree of

Doctor of Philosophy

California Institute of Technology

Pasadena, California

1971

(Submitted May 13, 1971)

ACKNOWLEDGEMENTS

I wish to thank Professor Felix Boehm for introducing me to the field of symmetry experiments in nuclear physics and for his guidance and encouragement in this work. I am indebted to Dr. J.C. Vanderleeden for sharing his experience in parity experiments, to Dr. P. Vogel for discussions on nuclear theory and to Mr. H.E. Henrikson for advice in the design of the apparatus.

This work was supported in part by the U.S. Atomic Energy Commission and the National Science Foundation.

ABSTRACT

Weak interaction theories of the "current-current" form predict a weak parity-non-conserving force between nucleons. One manifestation of such a force is the net circular polarization of γ rays from unoriented nuclei. We have measured the circular polarization for four favorable nuclear γ transitions obtaining

$$^{180}\text{Hf}\ 501\ \text{keV}\ \gamma: \quad P_\gamma = (-23 \pm 6) \times 10^{-4}$$
$$^{159}\text{Tb}\ 363\ \text{keV}\ \gamma: \quad P_\gamma = (-1 \pm 5) \times 10^{-4}$$
$$^{203}\text{Tl}\ 279\ \text{keV}\ \gamma: \quad P_\gamma = (-0.04 \pm 0.10) \times 10^{-4}$$
$$^{181}\text{Ta}\ 482\ \text{keV}\ \gamma: \quad P_\gamma = (-0.031 \pm 0.025) \times 10^{-4}$$

The measurements were performed with a forward-scattering rapidly-reversing Compton polarimeter and a phase-sensitive detection system. The analyzing efficiency of the Compton polarimeter, including effects of multiple scattering, was determined by Monte Carlo calculations. It was necessary in most experiments to apply corrections for polarized bremsstrahlung associated with β decays. Calculations of bremsstrahlung effects were verified by experiments on ^{198}Au and ^{177}Lu. The residual asymmetry of the polarimeter itself was determined by control experiments on ^{103}Ru.

The values of P_γ obtained are compared with related experiments and discussed in the framework of nuclear and weak-interaction theories.

To Carol

TABLE OF CONTENTS

APPENDICES

I. INTRODUCTION

I.1 General Introduction

Shortly after parity non-conservation (PNC) in the weak interactions was proposed [1] and subsequently discovered in β-decay experiments, [2] a weak interaction theory was put forward which stands today as the basis of more detailed theories. This "current-current theory" [3] predicts among other things a non-leptonic weak force between nucleons of strength $\sim 10^{-7}$ relative to the strong nuclear force. Such a force would give rise to parity admixtures in nuclear states and consequently pseudoscalar phenomena such as net circular polarization of γ rays from unoriented nuclei or a $P_1(\cos\theta)$ term in the angular distribution of γ rays from polarized nuclei.

Measurements of such non-leptonic PNC effects in nuclei furnish an important test of the current-current theory and provide quantitative information for detailed theoretical descriptions. The interpretation of measurements is complicated somewhat by uncertainties in nuclear structure effects, which must be known in order to unfold the weak interaction implications.

We describe in this thesis circular polarization measurements for four γ transitions, namely the 501 keV γ in ^{180}Hf, the 363 keV γ in ^{159}Tb, the 279 keV γ in ^{203}Tl and the 482 keV γ in ^{181}Ta. In these transitions (especially the first two) nuclear structure effects are expected to enhance the observable effects of parity mixing. Besides this condition there are a number of practical constraints which limit the nuclei feasible for such an experiment. Indeed other than the

cases above, only four others (343 and 396 keV γ's of ^{175}Lu, 1290 keV γ of ^{41}K and 401 keV γ of ^{75}As) have been attempted to date. Because of nuclear physics complications and because of the technical difficulty of the experiments themselves, it is important to study as many nuclei as possible and furthermore for several independent laboratories to confirm one another's results.

In such experiments the magnitudes P_γ of circular polarization (measured or predicted) are generally in the range 10^{-6} to 10^{-3}. The most practical techniques for analyzing γ-ray circular polarization is to measure an asymmetry for Compton scattering from electrons (in a magnet) polarized alternately in two opposite directions. Of the three alternative geometries [4] (a) transmission, (b) forward-scattering and (c) backward-scattering, we have chosen forward scattering because of its high intensity and analyzing efficiency. However, the efficiency is still only about 2% (i.e. measured asymmetries are only about 2% of P_γ, as explained in Appendix A).

The integral detection technique [5, 6] has been adopted here in order to surmount rate (and thereby statistical) limitations imposed by singles-counting techniques. The particular method employed in this experiment will be described fully in the next chapter.

A number of effects interfere with the measurement of P_γ. The main one is due to polarization of bremsstrahlung associated with the β decays (which are "semi-leptonic" PNC processes as opposed to the "non-leptonic" PNC processes we seek by measuring P_γ). In order to correct for this we have performed calculations and studied comparison cases (where P_γ should be negligible compared to bremsstrahlung effects)

namely ^{198}Au and ^{177}Lu. In order to determine any residual asymmetry in the Compton polarimeter we have performed control experiments with ^{103}Ru sources (negligible P_γ).

In the following section we outline the theoretical background for the parity experiments. For further details on theory and experiments the reader is referred to three recent review articles [7, 8, 9] and the references therein.

I.2 Theoretical Framework

(a) Weak Interaction Theory

The current-current theory proposed by Feynman and Gell-Mann [3] describes the weak interaction Hamiltonian H_w as the inner product of a current J_μ with itself

$$H_w = \sqrt{8}\ G\ (J_\mu\ J_\mu^{+} + \text{h.c.})$$

where the weak coupling constant $G = 1.0 \times 10^{-5}/M_p^2$, M_p being the proton mass. J_μ itself has in essence the form (for notation see Ref. 3):

$$J_\mu = (\bar{e}\nu_e) + (\bar{\mu}\nu_\mu) + (\bar{n}p) + (\bar{\Lambda}p) + \ldots$$

where

$$(\bar{e}\nu_e) = (\bar{\psi}_e\ \gamma_\mu\ (\frac{1 + i\gamma_5}{2})\ \psi_{\nu_e})$$

and similarly for $(\bar{\mu}\nu_\mu)$. The meanings of $(\bar{n}p)$ and $(\bar{\Lambda}p)$ are complicated somewhat by strong interaction effects. More generally we write

$$J_\mu = J_\mu^{\ell} + J_\mu^{h}$$

with ℓ for leptonic and h for hadronic. In the Cabibbo theory [10] J_μ is

further decomposed

$$J_\mu^h = J_\mu^{\Delta S=0} \cos\theta + J_\mu^{\Delta S=1} \sin\theta$$

where S is the strangeness and θ is the Cabibbo angle ($\sin\theta \approx 0.22$).

In forming H_w we note that in addition to cross-terms like $(\bar{n}p)(\bar{\nu}_e e)$ which account for β decay or $(\bar{\Lambda}p)(\bar{\nu}_e e)$ which account for hyperon decay, there are diagonal terms like $(\bar{n}p)(\bar{p}n)$ which indicate a weak N-N force.

In nuclei the contribution from this contact term shown diagrammatically in Fig. I.1 (a) is highly suppressed due to the hard core in the strong N-N interaction. Instead the finite range weak forces indicated in Fig.I.1(b) and (c) dominate.

Detailed considerations show that the $J_\mu^{\Delta S=0}$ term in J_μ^h gives rise to $\Delta I = 0, 2$ (where I is isospin) potentials only, physically corresponding to vector meson exchange (ρ, ω, φ), Fig. I.1(b). These exchanges enter with a factor $\cos^2\theta$.

On the other hand the $J_\mu^{\Delta S=1}$ current leads to $\Delta I = 1$ potentials corresponding to pseudoscalar meson (i.e.π) exchange, Fig. I.1(c), entering with a factor $\sin^2\theta$. Thus the Cabibbo theory suppresses the π relative to the ρ by a factor $\tan^2\theta \sim .05$. On the other hand the π by virtue of its longer range gets enhanced by the N-N hard core. There is considerable theoretical activity presently to determine the relative effects of π and ρ exchanges and to clarify the isospin structure of H_w and V^{PNC}. In this connection the problem of short-range N-N correlations (due to hard core) is receiving much attention. In

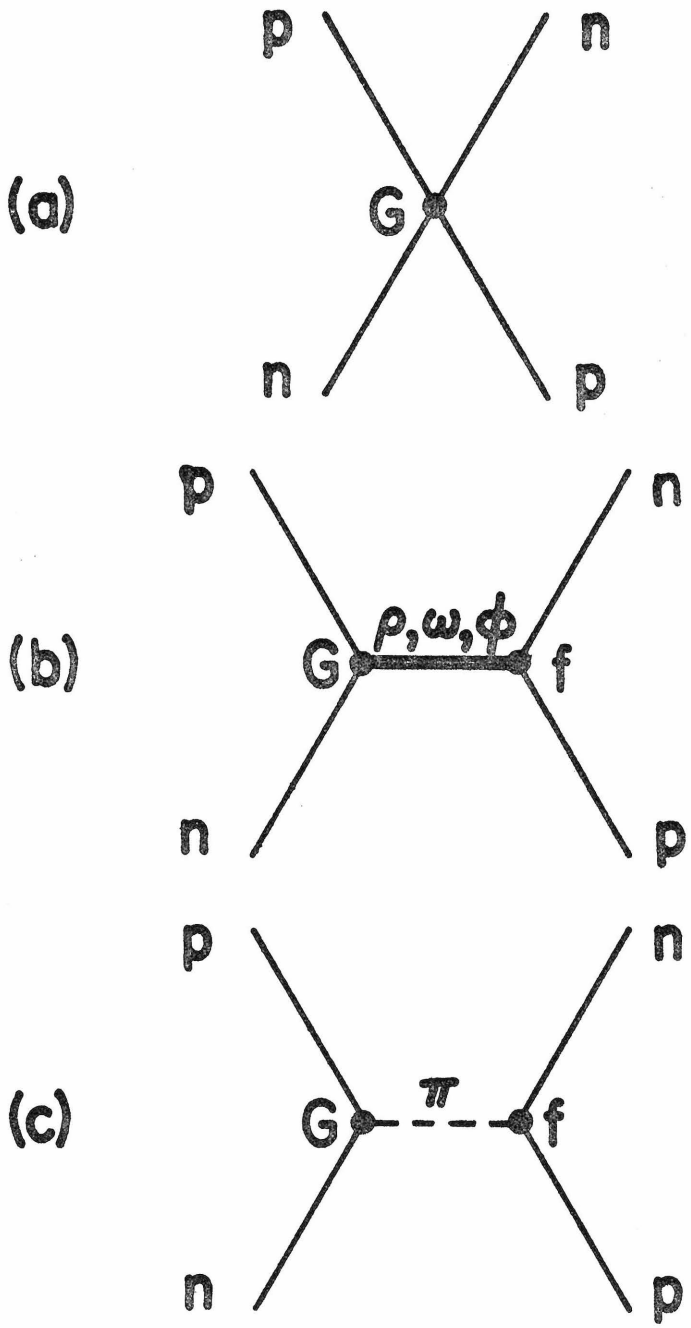

Fig. I.1 Non-Leptonic weak couplings (a) contact term, (b) vector meson exchange, (c) pseudoscalar meson exchange. Coupling constants G and f indicate weak and strong interaction vertices.

addition certain theoretical models ascribe "neutral currents" like $(\bar{p}p)$ to J_μ. To date such $\Delta I = 0$ currents are neither required nor excluded by experimental results.

(b) Parity Admixtures to Nuclear States

In practice the non-leptonic strangeness-conserving part of H_w is reduced to an effective pseudoscalar nuclear potential V^{PNC}. Some theoretical workers deal with an internucleon potential while others reduce it further to a single-particle form $\vec{\sigma} \cdot \vec{p}V(r)$. Generally V^{PNC} may include both static and velocity dependent terms. V^{PNC} is treated as a perturbation to the strong nuclear Hamiltonian. The modification to the parity pure states φ_i of energy E_i is given by

$$\psi_i = \varphi_i + \sum_{j \neq i} \frac{\langle \varphi_j | V^{PNC} | \varphi_i \rangle}{E_i - E_j} \varphi_j \quad .$$

If state φ_i has spin and parity J^π then only those φ_j with $J^{-\pi}$ will contribute.

(c) Resultant Circular Polarization of γ Rays

Consider a γ transition between two states ψ_1 and ψ_2 and let us assume for example that the parity mixing is dominated by only one unperturbed state φ' which mixes into the initial state. Then

$$\psi_1 = \varphi_1 + \frac{\langle \varphi' | V^{PNC} | \varphi_1 \rangle}{\Delta E} \varphi'$$

where $\Delta E = E_1 - E'$ and

$$\psi_2 = \varphi_2$$

Suppose that the regular γ transition between φ_1 and φ_2 is of character E1-M2; then the irregular transition between φ' and φ_2 will be mostly $\widetilde{M1}$ (we emphasize with the tilda that this is the irregular transition).

Then the circular polarization will be[11)]

$$P_\gamma = \frac{2}{1+\delta^2} \quad \frac{\langle \widetilde{M1} \rangle}{\langle E1 \rangle}$$

where $\delta = \frac{\langle M2 \rangle}{\langle E1 \rangle}$, the mixing ratio of the regular transition, and $\langle E1 \rangle$ and $\langle \widetilde{M1} \rangle$ are the reduced matrix elements of the multipole operators O(E1) and O(M1)

$$\langle E1 \rangle \equiv \langle \psi_2 || O(E1) || \psi_1 \rangle$$

$$= \langle \varphi_2 || O(E1) || \varphi_1 \rangle$$

$$\langle \widetilde{M1} \rangle = \langle \psi_2 || O(M1) || \psi_1 \rangle$$

$$= \langle \varphi_2 || O(M1) || \varphi' \rangle \frac{\langle \varphi' | V^{PNC} | \varphi_1 \rangle}{\Delta E}$$

More generally

$$P_\gamma = 2 \frac{\sum_L \langle ML \rangle \langle EL \rangle}{\sum_L (\langle ML \rangle^2 + \langle EL \rangle^2)}$$

Note that there is no direct interference between different multipole orders (like E1-$\widetilde{E2}$).

For most γ transitions P_γ is too small to measure, but in certain favored nuclei, such as those investigated in this study, one may

reasonably expect a large P_γ due to a small ΔE and/or strongly hindered regular transitions.

II. EXPERIMENTAL METHOD

II.1 Introduction

In order to analyze circular polarization we take advantage of the dependence of the Compton scattering cross section on the relative polarizations of the photon and electron.[4,12] The basic idea is that a photon of given polarization (±1) will have a different probability of scattering off an electron and into the detector if the electron spin is forward or backward. A convenient source of polarized electrons is a ferromagnet, although at saturation in iron alloys generally only 6-8% of the electrons participate.

In Fig. II.1, we show our Compton polarimeter; γ rays originating in the source material within the titanium capsule scatter off electrons in the inner region of the magnet and are detected by the coaxial lithium-drifted germanium detector. By measuring the relative change in detector current as the magnetization(mean electron spin)is reversed we are able to deduce the γ ray circular polarization.

In this experiment we adopt the integral detection technique proposed by Lobashov.[5] By measuring the detector current rather than counting single pulses, we sacrifice energy resolution in favor of high counting rates.

Letting I_+ (I_-) denote the detector current when the electron spins are forward (backward), we define the asymmetry

$$A = \frac{I_N}{I_D}$$

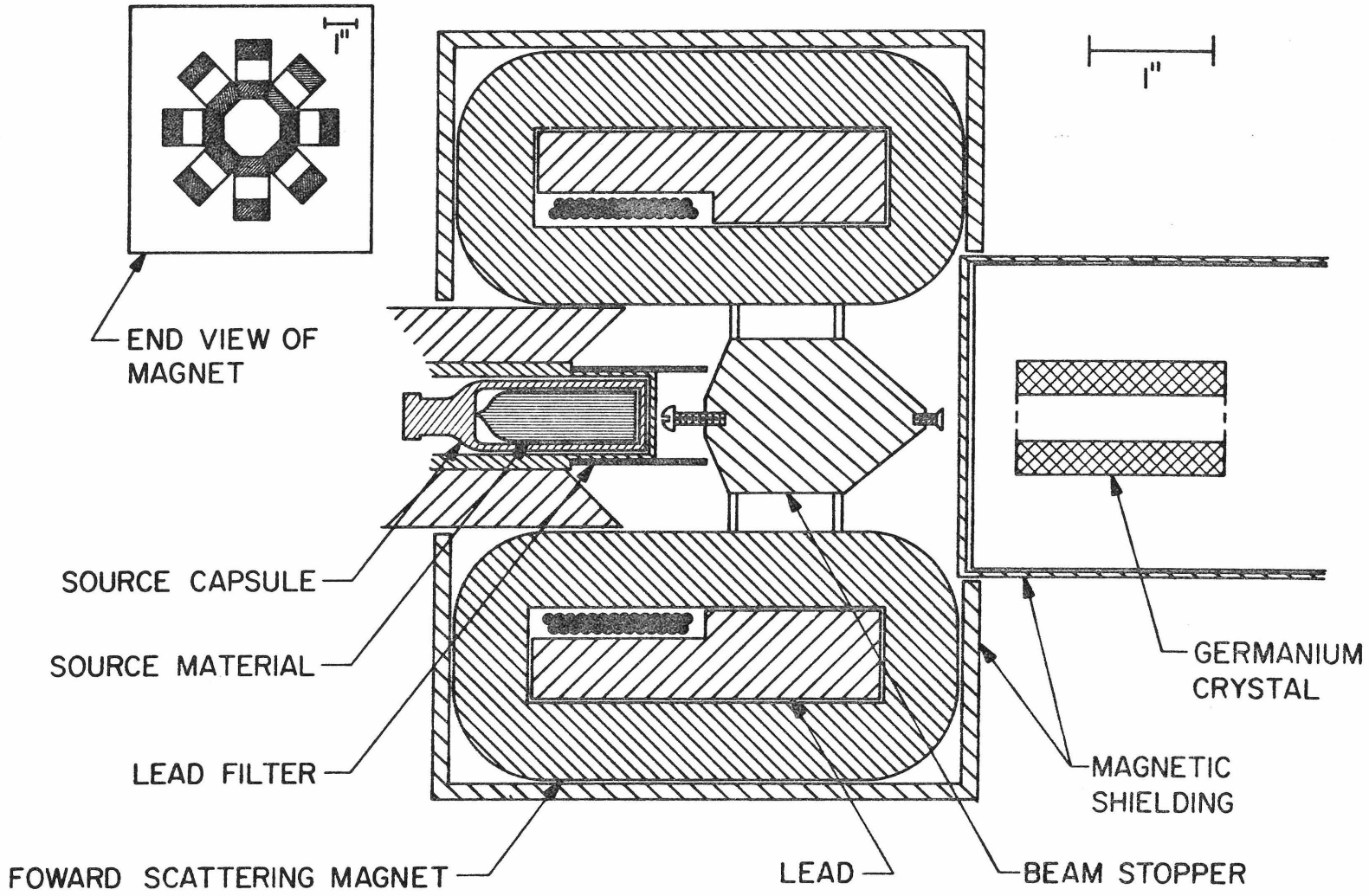

Fig. II.1 The Compton Polarimeter

where N stands for numerator and D for denominator with $I_N = (I_- - I_+)/2$ and $I_D = (I_- + I_+)/2$.

In general I_N and I_D will have contributions other than from the γ ray of interest. I_D will include other rays and I_N will include a term from polarized bremsstrahlung associated with any β decays in the source.

In Appendix A,we first derive a general expression for the asymmetry A in terms of the intensity and polarization of the β bremsstrahlung and γ rays. Then we outline the Monte Carlo calculation of the polarimeter efficiency functions which appear in the expression for A. In Appendix B we describe the internal (IB) and external (EB) bremsstrahlung calculations. With the machinery of Appendices A and B we are then able to unfold the γ polarization P_γ from an observed asymmetry A.

A block diagram of the system is shown in Fig. II.2. In the next two sections, the details of the system are presented.

II.2 The Compton Polarimeter

The analyzer for circular polarization (Fig. II.1) was a forward scattering magnet assembled from eight rectangular cores wound from a 4-mil tape of grain oriented silicon iron.[13] The purpose of such laminated material is to suppress eddy currents and thereby permit fast switching. After winding, the cores had been annealed and them impregnated with varnish for strength. In our shop the eight cores were beveled on two edges at $22\frac{1}{2}°$ on a surface grinder to permit a rigid close-packed octagon formation (see insert on Fig. II.1). The cores were cemented together with the help of a cylindrical octagon form in the center.

After the 25 turn coil was wound, the magnet was placed in a

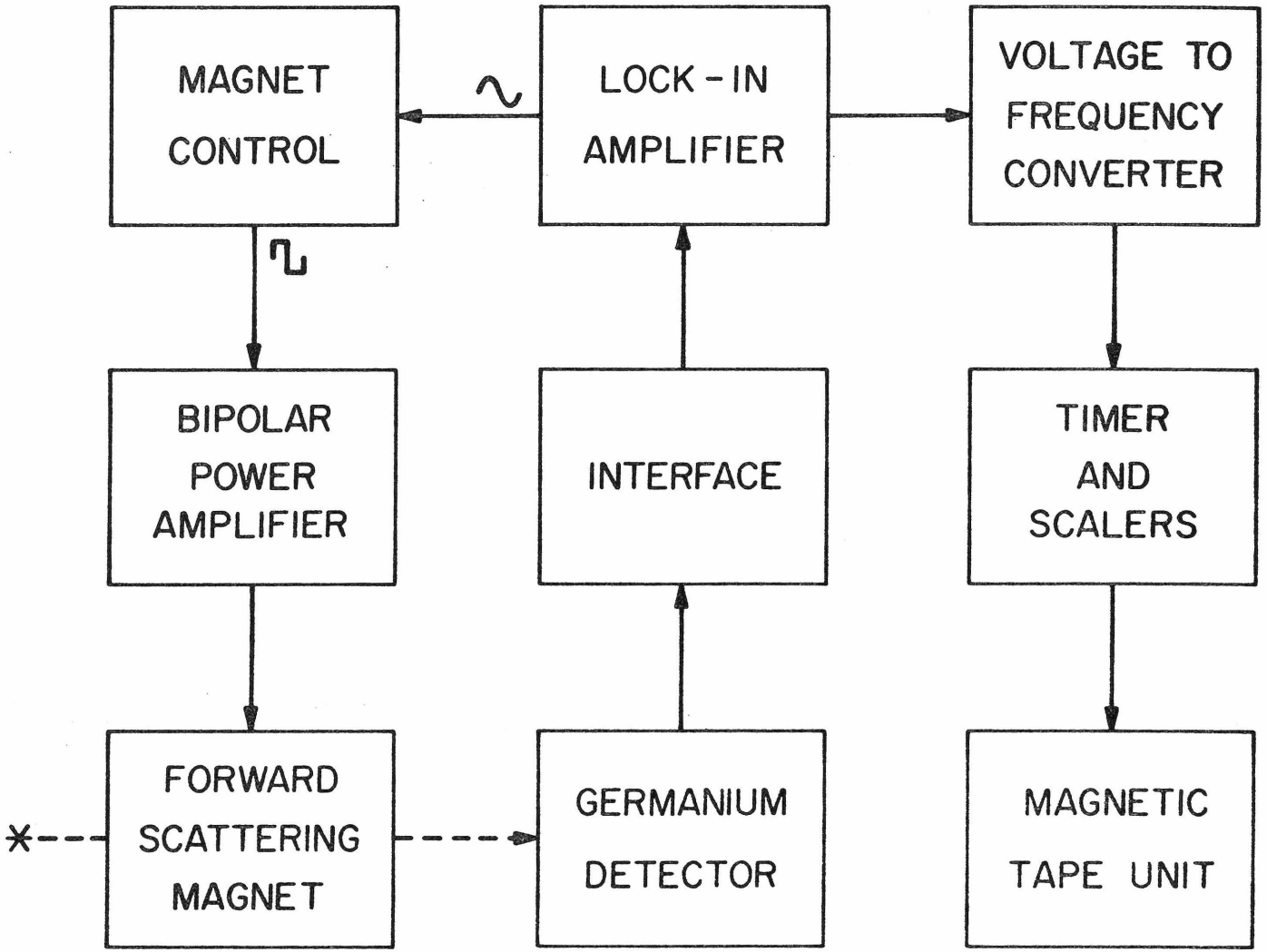

Fig. II.2 Block diagram of system.

cylindrical aluminum shell and fixed with set screws. A sandwich of magnetic shielding foils[14] alternated with aluminum foils was fastened with epoxy resin to the outside of the shell and the endcaps, in order both to contain the magnet's 10Hz stray fields and to help isolate the magnet from the earth's magnetic field (see Sec. II.6(g)).

The magnet current $I^M = \pm 5$ A produced a magnetic field $H = \pm 6.5$ Oe and saturation induction $B = \pm 17.5$ kG. The magnetization was reversed in 7.4 msec. The Magnet Control circuitry, shown in Fig. II.3, converts the 10Hz reference sine-wave from the lock-in amplifier into a precision square wave for which the amplitude and time symmetries are adjustable. The importance of these symmetries is discussed in Appendix C. The square wave is then delivered to the bipolar power amplifier which is programmed by external feedback components to deliver ± 5 A to the magnet, except during reversal when the output voltage clamps at ± 39 V. By Faraday's law, B then reverses linearly in time. Thus during reversal the waveform of I vs t is, aside from scale factors, equivalent to a waveform of H vs B, i.e. a hysteresis curve on its side. (To monitor this we temporarily disconnected the damping resistor which, besides fulfilling its function of suppressing ringing, draws ± 2.4 A during reversal.) This feature was useful in monitoring the dynamic hysteresis and, for example, selecting the number of turns. The magnet waveforms are shown in Fig. II.4(a).

The fraction of polarized electrons at B = 17.5 kG was calculated to be $f_0 = .067$ based on the formula

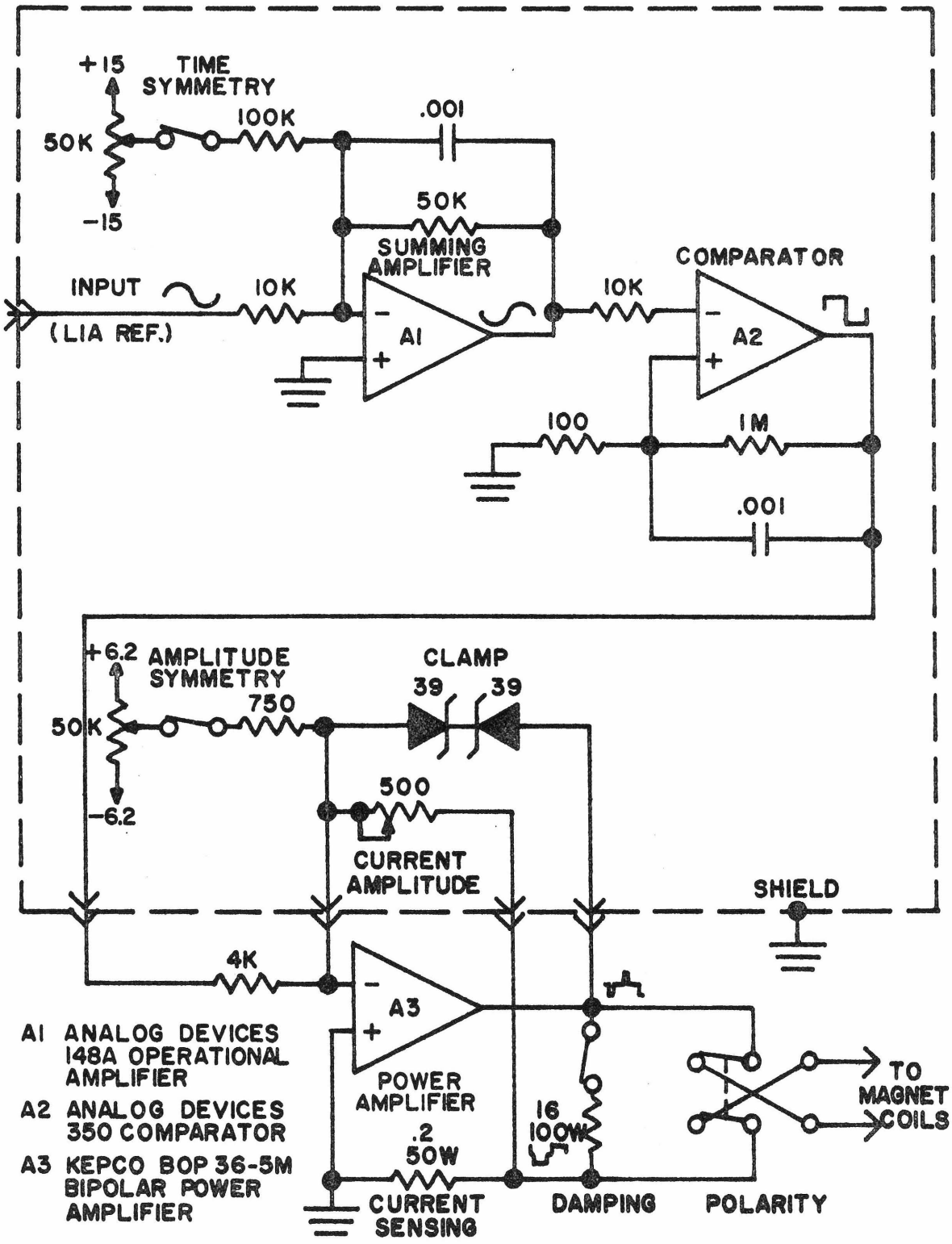

FIG. II.3 Magnet control circuits

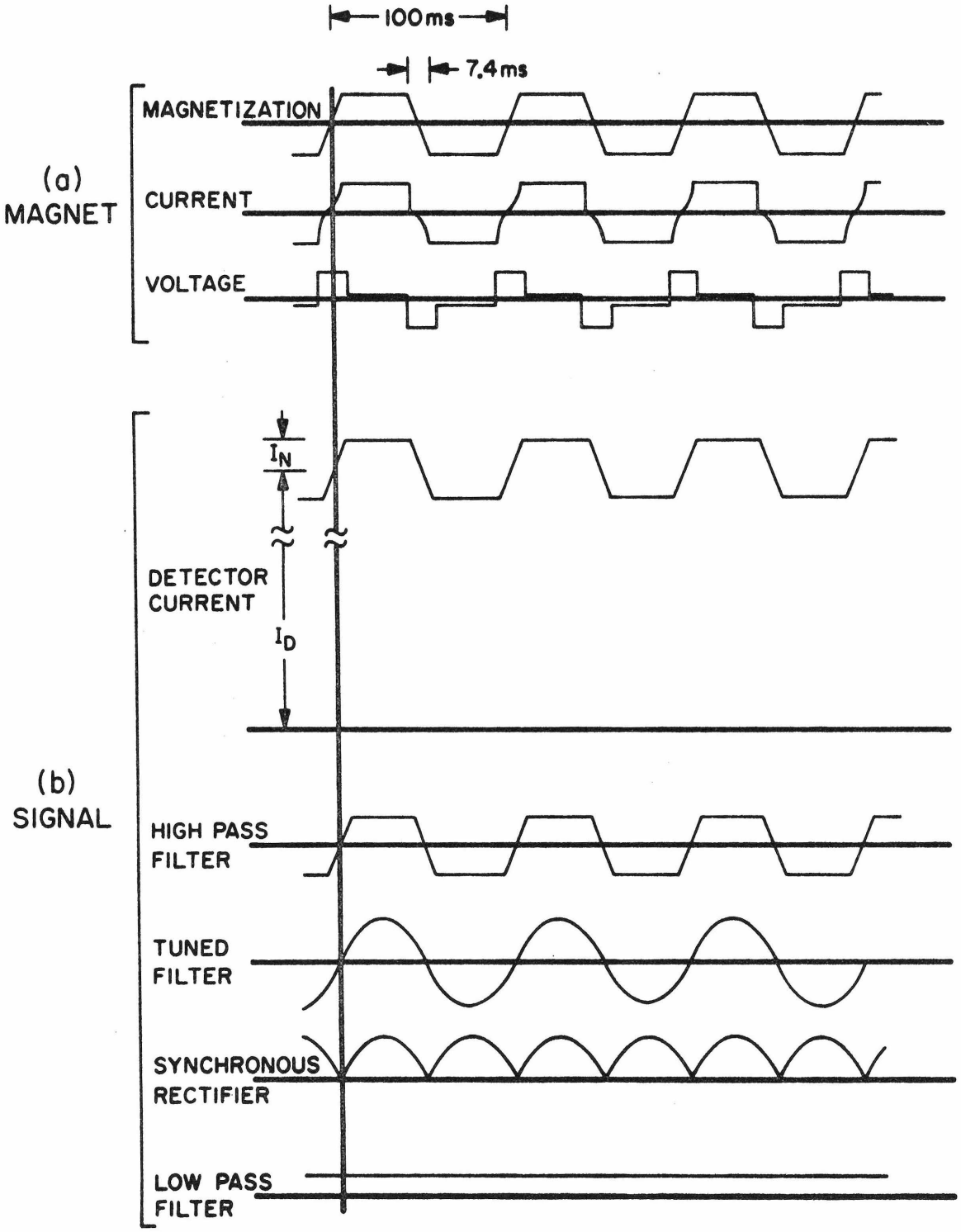

Fig. II.4(a) Magnet waveforms, (b) filtering and demodulation of signal waveform.

$$f_0 = \frac{B}{4\pi\mu_B} \cdot \frac{2}{g} \cdot \frac{1}{n^e_{Fe} + n^e_{Pb}}$$

where $g \approx 2.07$ is the gyromagnetic ratio for Fe; $n^e_{Fe} = 2.08 \times 10^{24}$ cm^{-3} and $n^e_{si} = 0.07 \times 10^{24}$ cm^{-3} are the electron densities for the Fe and Si in the silicon-iron.

II.3 Phase Sensitive Detection System

As a consequence of a net γ ray circular polarization the detector current I_D was modulated by a tiny 10 Hz square wave of amplitude I_N proportional to the degree of circular polarization.

I_D, which had negligible fluctuations, was measured during the course of each experiment by connecting a differential voltmeter across the load resistor (see Fig. II.5). In the experiments I_D ranged from 10 nA to 100 μA and was corrected when necessary for leakage and dark currents which amounted together to about 0.5 nA.

I_N, which was buried in noise mainly from the randomness of the source decay, was separated from I_D by A.C. coupling and passed to the remote preamplifier of the lock-in amplifier[15] (LIA) for phase sensitive demodulation. The "interface" circuitry between the detector and LIA is detailed in Fig. II.5. The filter passband is roughly 1 Hz to 100 Hz.

The method by which the LIA performs its phase sensitive detection is indicated in Fig. II.4(b). The high-pass filter blocks the D.C. and the tuned filter (Q = 5) suppresses harmonics. Then comes the synchronous rectifier which in effect multiplies the noisy signal by a unit amplitude square wave derived from the LIA reference sine wave.

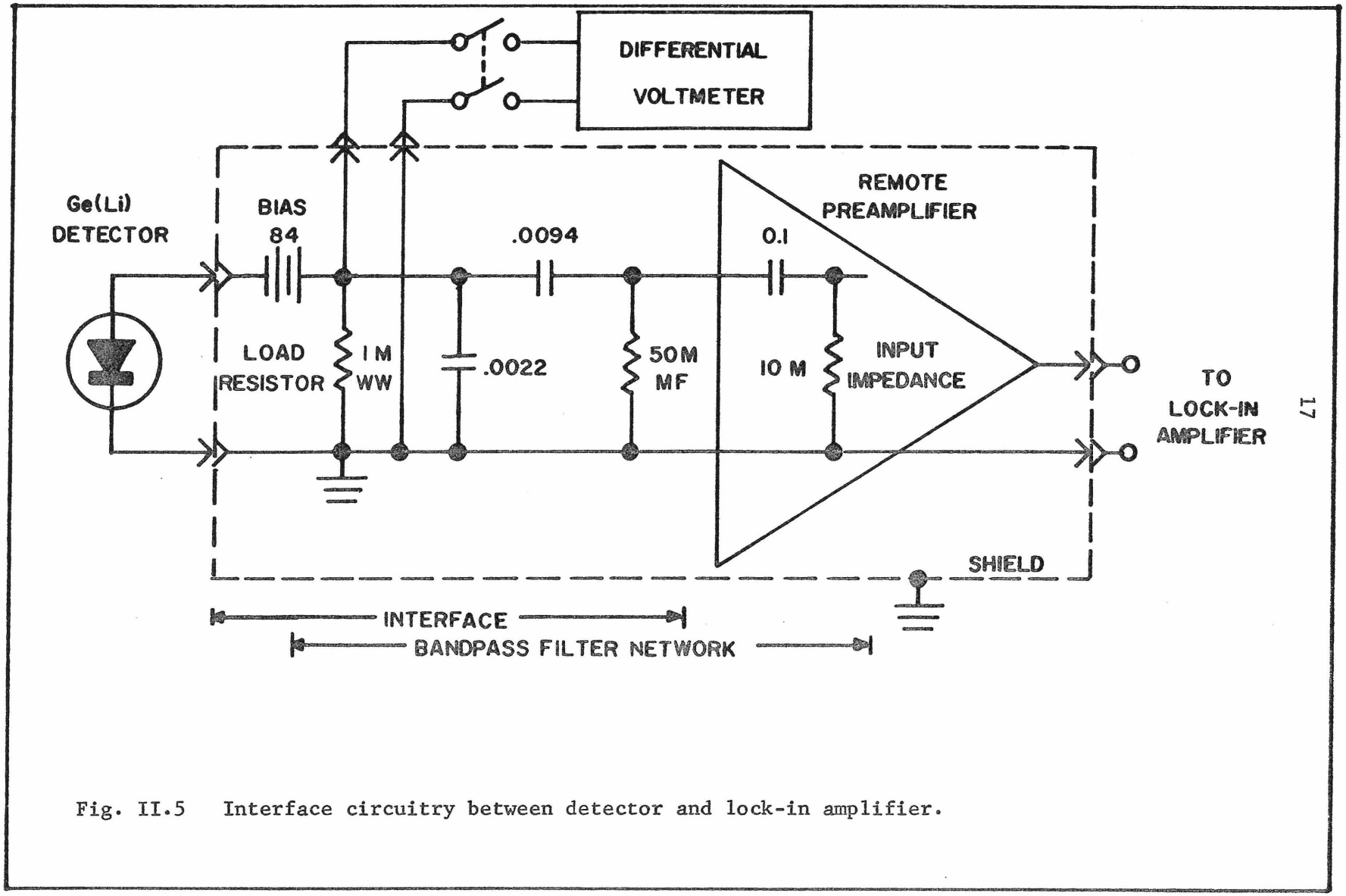

Fig. II.5 Interface circuitry between detector and lock-in amplifier.

Thus the fundamental (and the residual odd harmonics) are rectified whereas the noise is effectively unrectified. Finally the noise and rectified signal are averaged by a two stage low pass filter with 100 sec time constant. The LIA output is averaged by a bipolar voltage-to-frequency converter [16] (VFC) and a pair of 6-digit scalers which are read out every 100 sec onto a magnetic tape for subsequent computer analysis.

The LIA is calibrated in terms of the RMS of the fundamental of our signal which is in fact a trapezoid. To convert this RMS to the effective square wave amplitude involves a factor

$$\sqrt{2}\,\frac{\pi}{4}\,\frac{\sin(\omega_0 T_s/2)}{(\omega_0 T_s/2)} = 1.12$$

with $\omega_0 = 2\pi \times 10$ Hz and $T_s = 7.4$ ms, the reversal time. The correction for loading effects in the filter network in the "interface" requires an additional factor 1.15. Lastly there is a factor 0.99 to correct for third harmonic pickup.

The phase shifts of the system components were measured or calculated. The overall phase shift was adjusted to less than 3° corresponding to a negligible signal attenuation of less than (1- cos 3°) = 0.1%. In all we must multiply the LIA output by a factor $1.12 \times 1.15 \times 0.99 = \underline{1.28}$ to obtain the equivalent square wave amplitude I_N.

II.4 Data Analysis Procedures

Each experiment consisted of a series of runs, typically ten. The raw data included manual measurements of I_D at the beginning and end of each run as well as successive readouts on magnetic tape every 100 sec

of the (+) and (-) scalers. As mentioned above the difference of these scaler readings is proportional to the LIA output which in turn is a measure of I_N. The successive readouts every 100 sec (determined by capacity of scalers) were strongly correlated by the 100 sec time constant of the LIA output amplifier. To obtain negligibly correlated (< 1%) data, the readouts were averaged further by computer in groups of 16 (equivalent to reading out every 1600 sec). We determined empirically that data analysis using 100 sec intervals (as if independent) lead to an error underestimated by a factor 1.92. (For some early data which had been analyzed naively with 100 sec intervals, the calculated errors were increased a posteriori by this factor 1.92.)

For long-lived cases such as ^{181}Hf and ^{103}Ru with $T_{1/2} \gg T_{RUN}$ (the run times T_{RUN} were $\lesssim$ 5 days here), the data within each run were analyzed as follows. Let M be the number of (grouped) readouts $I_{N,m}$ of I_N. Then the mean was $\overline{I_N} = \frac{1}{M}\sum_{m=1}^{M} I_{N,m}$ with error $\sigma_{\overline{I}_N} = [(\overline{I_N^2} - \overline{I}_N^2)/(M-1)]^{1/2}$; note the neglect here of statistical weighting of the $I_{N,m}$ to allow for source decay. $\overline{I_D}$ was taken simply as the mean of the two measurements at the beginning and end of the run (negligible bias $\simeq .04\ (T_{RUN}/T_{1/2})^2$). The error for $A = \overline{I_N}/\overline{I_D}$ was taken as $\sigma_A = \sigma_{\overline{I}_N}/\overline{I}_D$. Finally such results A_i, σ_{A_i} of separate runs under identical conditions were combined to give $A = (\Sigma A_i/\sigma_{A_i}^2)/(\Sigma 1/\sigma_{A_i}^2)$ with $\sigma_A = 1/(\Sigma 1/\sigma_{A_i}^2)$.

For short-lived cases such as $^{180}Hf^m$ and ^{159}Gd we analyzed I_N and I_D to allow for source decay. In these sources as well as in the surrounding titanium-metal capsule there were often a few isotopes contributing significantly to I_N and/or I_D. Generally, suppose there

were K isotopes contributing to $I_N(t)$ with lifetimes τ_k (reserve k = 1 for the isotope of interest). Then $I_N(t)$ was fit by least squares to determine $I_N^k(0)$ (and its error) in

$$I_N(t_m) \sim \sum_{k=1}^{K} I_N^k(0)\, e^{-t_m/\tau_k} \quad .$$

In this fit we incorporated statistical weights for $I_N(t_m)$ given by $\frac{1}{\sigma^2_{I_N(t_m)}} \propto \frac{1}{I_D(t_m)}$. The last relation is the extension to our integral detection method of the familiar "square root of the number of counts" rule for the error in singles-counting experiment. An analytic form for $I_D(t_m)$ was obtained from the fit for $I_D(t)$ discussed next. In the final analysis for the $I_N^k(0)$ for each experiment, all runs were effectively recombined as if there were one continuous run (with gaps). Similarly $I_D(t)$ was fit for L isotopes of lifetimes τ_ℓ (generally a slightly different set than the τ_k; again ℓ = 1 for the isotope of interest). Then the values $I_D(t_j)$ were fit to determine $I_D^\ell(0)$ in

$$I_D(t_j) \sim \sum_{\ell=1}^{L} I_D^\ell(0)\, e^{-t_j/\tau_\ell}$$

with no statistical weighting since the $I_D(t_j)$ fluctuated negligibly during the manual measurements.

In practice K was 1 or 2 and L was 1, 2 or 3. In some cases we used the I_D fit to help identify contaminants by observing what value of τ_3, say, would give a minimum of the goodness-of-fit parameter χ^2 for given τ_1 and τ_2. This information was complemented by γ spectra of the sources before and after the experiment.

The final asymmetry for the experiment (referred to the isotope of interest) was $A = I_N^1(0)/I_D^1(0)$ with $\sigma_A = \sigma_{I_N^1(0)}/I_D^1(0)$; the percentage error in $I_D^1(0)$ was always negligible compared to that of $I_N^1(0)$.

II.5 Source Selection and Design

There are a number of constraints which limit the cases feasible for this type of experiment. To begin with, we want a γ ray of energy in the range 0.2 to 1.2 MeV for which we may reasonably expect an enhanced circular polarization. We are encouraged in particular if there happen to be any opposite parity states near the initial or final states and if the regular multipole transition is hindered.

The γ ray must have sufficient relative and absolute intensity. Any associated β decay must not be of such high energy that the bremsstrahlung would overwhelm the expected asymmetry for the γ. The virtue of the preceding β decay is to give the source a practicable lifetime. Only in $^{180}Hf^m$ did we avoid the need for a β-decaying parent.

We must be able to produce sufficient activity of the parent isotope. For example if we desire to resolve an asymmetry 3×10^{-8}, then we will need $\sim 10^{15}$ detected events or $\sim 10^{18}$ from the source. If we want to run two weeks ($\sim 10^6$ sec), then we need at least 10^{12} γ's per second or 30 Ci of the γ . To produce such activities we are restricted to thermal neutron capture. Thus to produce the parent isotope (Z,A) we need a stable isotope (Z, A-1), with sufficient abundance and cross section to activate the material we can accomodate in the 4 cm^3 capsule. Finally we must ensure that other isotopes in the material do not produce enough activity to obscure our effect because of bremsstrahlung or γ intensity.

In order to mitigate some of these constraints, we sometimes used enriched material (higher activity, less contaminants) and/or diluted the sources with carbon powder (suppresses external bremsstrahlung).

In addition to parity cases we used ^{177}Lu and ^{198}Au as checks on the calibration and bremsstrahlung calculations. For controls we used ^{103}Ru. The dominant 497 keV γ ray in this decay is unhindered ($\tau \sim 100$ psec) and expected to show negligible polarization.

The details on our sources are tabulated with the results in Chapter III. After preparation the source material was enclosed in welded titanium [17] capsules. In a few cases for which we wanted less volume than the 4 cm^3, the source powder was enclosed in an inner vial of pure quartz.

II. 6 Systematic Errors

It is not surprising that in seeking an asymmetry $A \lesssim 10^{-6}$ we are vulnerable to a number of phenomena that may imitate or distort this effect. In order to eliminate such "false asymmetries" or at least determine their magnitude , we have performed a number of control measurements. We now consider in turn the various causes and relative importance of these false asymmetries:

(a) Bremsstrahlung

In all cases except ^{180}Hf^m the γ is fed from a β-decaying parent. The internal (IB) and external (EB) bremsstrahlung following these β decays, although weak in intensity is highly circularly polarized and will thus contribute to A via I_N. In cases where (the β endpoint T_β) $\lesssim$ (the γ energy k), the bremsstrahlung could be suppressed somewhat by lead filters (Fig. II.2).In any case the EB could be reduced by a

factor $\lesssim 10$ by diluting the source material with a low Z material like carbon. We have calculated IB and EB intensities and polarizations for our cases and checked the calculations with ^{177}Lu and ^{198}Au. The role of bremsstrahlung in the asymmetry is indicated in Appendix A while the calculations themselves are described in Appendix B. The IB and EB results in each case are given in Chapter III.

(b) Contaminants

Radioactive isotopes other than the one of interest may be present in significant amounts either in the source material (from isotopes of the same element or chemical impurities) or in the capsule. Generally their γ rays will be practically unpolarized and will contribute to I_D only; on the other hand any bremsstrahlung will contribute to I_N. Contaminants notably in the cases of ^{180}Hf and ^{159}Tb are discussed in Chapter III.

(c) Source Decay

In experiments (unlike this one), which have D.C. coupling throughout, source decay between magnet reversals can introduce an apparent asymmetry. These effects can be suppressed somewhat by using a complex switching pattern.[18] However in our A.C. experiment the high frequency (10 Hz) and the various filters (high-pass, band-pass, synchronous-rectifier) serve to attenuate these effects such that even in the worst case of 5.5 hr ^{180}Hf^{m} the contribution of source decay to the asymmetry would be $< 10^{-10}$, i.e. negligible. (With 10 Hz and D.C. coupling the false asymmetry would be $\sim \lambda\Delta t = \frac{\pi \ell n 2}{\omega_0 T_{1/2}} \sim 10^{-6}$).

(d) Right-Left Asymmetry

Bock[19] has measured an asymmetry apparently of the form

$R\ \vec{s} \cdot \vec{k}_1 \times \vec{k}_2 / |\vec{k}_1 \times \vec{k}_2|$ where $\vec{s}$ is the electron polarization and $\vec{k}_1$ and $\vec{k}_2$ are the initial and final photon momenta. Using a spare rectangular magnet core and a source of ^{103}Ru with γ energy k = 497 keV, we verified Bock's early measurements obtaining $R = (1.7 \pm 0.2) \times 10^{-3}$ at $\theta = 45°$ (resolution $\Delta\theta = 10°$) and $R = (-0.7 \pm 0.1) \times 10^{-3}$ at $\theta = 85°$ ($\Delta\theta = 20°$). More recently Bock has reconsidered these effects and interpreted them as due in large part to double scattering.[20)]

In the parity experiment $\vec{s}$ is almost in the plane of $\vec{k}_1$ and $\vec{k}_2$ and the effect is reduced; moreover the non-coplanarities tend to cancel when averaged over the geometry. However, slight misalignments or non-homogeneities may lead to a non-zero resultant asymmetry for our polarimeter.

(e) Quadratic Effects

These effects, discussed in detail in Appendix C, arise from non-linear polarization dependence of absorption and multiple scattering processes. For monochromatic γ's (from the source) with circular polarization P, the detector current may be written

$$I = I_o\ (1 + L\ P\ f + Q\ f^2)$$

where the linear and quadratic coefficients L and Q are dependent on the γ energy and the polarimeter properties. The "normal" linear term permits our measurement of P. Here we call attention to the quadratic term which is independent of P. This gives rise to "false asymmetries" only if the magnetization waveform is asymmetrical in amplitude or time. For further discussion and numerical results see Appendix C.

(f) Magnetostriction and Motion

The dimensions of the magnet vary with magnetization according to the process of magnetostriction. In addition there may be relative motions of parts of the system because of magnetic forces. In either case a slight difference in effective solid angles for the two states would lead to a false asymmetry.

The silicon-iron for the magnet was chosen in part for its low magnetostriction coefficients.[21] If the magnet waveform is symmetrical there should be no false asymmetry from magnetostriction, Otherwise the effects would be similar to the quadratic effects (e). In fact the agreement between calculations and measurements in Appendix C indicate that the magnetostrictive effect is considerably smaller than the quadratic effect.

As for mechanical motions, successive refinements in the rigidity of the magnet support as well as measurements with an electromechanical transducer indicated these to be negligible.

(g) Earth's Magnetic Field

Although our polarimeter was oriented (geographically) east-west there was still a tiny component $\vec{H}_{e}^{\parallel}$ of the earth's field along the magnet direction. Thus for equal currents, H (and thus B) will be slightly different in the two states and we can get asymmetries from the quadratic effects (e). Improving the magnetic shield for the magnet and increasing the number of turns (equivalently H_{max}) did not appreciably affect the control asymmetry. So we conclude that this effect is negligible.

(h) Magnetic Pickup, Ground Loops and Output Offset

Pickup of the magnetic stray field in the detector or subsequent electronics, or other crosstalk between the "reference" and "signal" channel will contribute in effect to I_N. The Ge(Li) type of detector was chosen specifically for its insensitivity to magnetic fields. The critical circuits and the magnet were electromagnetically shielded and carefully grounded. It was easy to monitor any residual pickups since we could determine these without a source. In fact they were negligible.

Finally if the zero offset of the LIA output amplifier or the VFC drift out of adjustment they will contribute to I_N. These were checked periodically and found to be negligible.

(i) Conclusion: Observed Residual Asymmetry

With ^{103}Ru sources (497 keV γ) we did observe a net asymmetry $|A_{Ru}| \sim 0.2 \times 10^{-6}$ after a small correction for bremsstrahlung. This A_{Ru} was clearly not due to effects (a), (b), (c) or (h), since the effect did in fact depend on the presence of a beam of γ's. The fact that A_{Ru} was odd (like the A from polarized γ's) under the operation of reversing the magnetic polarity (see switch in Fig. II.3) relative to the reference waveform, indicated that A_{Ru} was not due to (e) or magnetostriction in (f). As we have ruled out the motion in (f), and (g) we strongly suspect (d), the right-left asymmetry. We tried several assemblies of the magnet pieces. Each time we got $|A_{Ru}| \lesssim 0.3 \times 10^{-6}$ with either sign. Finally after about five such efforts we abandoned the effort to eliminate (d). We accepted the fact that we have to live with a final reproducible value of $A_{Ru} = (-0.20 \pm 0.03) \times 10^{-6}$.

III. RESULTS

III.1 Introduction

The observed asymmetries and corresponding circular polarization results are presented for the four nuclei ^{180}Hf, ^{159}Tb, ^{203}Tl and ^{181}Ta in which we have studied effects of parity non-conservation. In addition we give results for ^{198}Au and ^{177}Lu, which were employed as checks on the bremsstrahlung and efficiency calculations, and for ^{103}Ru which was used to determine the background asymmetry of the polarimeter.

The experimental particulars on all sources are given in Table III.1. The results of bremsstrahlung and efficiency calculations are given for reference in Table III.2. The final results for all cases are summarized in Table III.3.

III.2 Application of Efficiency and Bremsstrahlung Calculations

In Sec. A.1 of Appendix A, we present the framework for expressing the experimental asymmetry A in terms of the bremsstrahlung (IB and EB) spectra and polarizations, the γ intensities and the polarization of γ_1 (the unknown). In Sec. A.2 we outline the Monte Carlo evaluation of the efficiency functions $D_n(k)$ with the parameter w, the lead filter thickness. In Appendix B we describe the bremsstrahlung calculations with one unknown parameter ζ to be divided into the preliminary EB($\zeta = 1$) intensity. The factor ζ is introduced to compensate for the zigzag trajectory of β particles in collisions preceding the EB event. The form of ζ is $\left\langle \frac{ds}{dr} \right\rangle$ (the nature of this average is defined in Appendix B) where s denotes the path length and r the net displacement. As we will see in Sec. III.3(b) we have determined $\zeta = 1.5$ for ^{198}Au (undiluted). Application of this value of ζ to the EB cal-

Table III.1 Descriptions of sources used in experiments.

Case	Daughter Isotope	Parent Isotope	Half Life	Initial Stable Isotope	Thermal Neutron Cross Section	Stable Isotope Abundance[a] (%)	Mass of Parent Element (g)	Chemical Form[b]	Mass of Carbon Diluent (g)	Number of Sources	Approx. Activity[c] (Curie)	Purpose
1	^{103}Rh	^{103}Ru	40d	^{102}Ru	1.4	32 N	10	Ru	0	3	100	Control
2	^{177}Hf	^{177}Lu	6.8d	^{176}Lu	2100	2.6 N	1	Lu_2O_3	2	1	100	Brems.
3	^{203}Tl	^{203}Hg	47d	^{202}Hg	3	30 N	7	HgO	0	1	100	Parity
4	^{181}Ta	^{181}Hf	43d	^{180}Hf	12	98 E	0.3	HfO_2	0.6	1	50	Parity
5a	^{180}Hf	$^{180}Hf^m$	5.5h	^{179}Hf	.34	14 N	50	Hf(ROD)	0	1	1	Parity
5b	^{180}Hf	$^{180}Hf^m$	5.5h	^{179}Hf	.34	14 N	15	HfO_2	0	5	1	Parity
6a	^{180}Hf	$^{180}Hf^m$	5.5h	^{179}Hf	.34	75 E	.75	HfO_2	0	5[d]	1	Parity
6b	^{180}Hf	$^{180}Hf^m$	5.5h	^{179}Hf	.34	58 E	1	HfO_2	3	3[d]	1	Parity
7	^{198}Hg	^{198}Au	2.7d	^{197}Au	99	100 N	0.1	Au_2O_3	3	1	30	Brems.
8	^{198}Hg	^{198}Au	2.7d	^{197}Au	99	100 N	2	Au_2O_3	0	1	30	Brems.
9	^{159}Tb	^{159}Gd	18.6h	^{158}Gd	3.5	92 E	0.1	Gd_2O_3	3	3	1	Parity.

[a] E denotes enriched isotope; N denotes natural abundance.

[b] Physical form is powder, unless otherwise noted.

[c] The irradiations in cases 1-4 were in a neutron flux of 4×10^{14} $cm^{-2}sec^{-1}$ at the ETR in Arco, Idaho; those in cases 5-9 were in a flux of 1.2×10^{14} $cm^{-2}sec^{-1}$ at the GETR in Pleasanton, California.

[d] Successive irradiations of one sample in each case.

Table III.2 Results of asymmetry calculations [a]

Case	Parent Isotope	Chemical Form	Dilution	Effective Z	Filter Thickness w(mm)	Denominator x 10^3	$-A_{IB} \times 10^6$	$-A_B \times 10^6$	$\frac{A_\gamma}{P_{\gamma 1}} \times 10^2$	$\frac{A_{\gamma 1}}{P_{\gamma 1}} \times 10^2$	Energy of γ_1 (keV)
1	$^{103}_{44}Ru$	Ru	-	44	0	1.77	.055	.101	(1.92)	(2.05)	(497)
					1	1.42	.031	.054	(1.85)	(1.98)	
					2	1.08	.023	.037	(1.81)	(1.95)	
2	$^{177}_{71}Lu$	Lu_2O_3	1:2	22	0	.075	6.6	8.3	(1.42)	(1.47)	(208)
					1	.022	8.3	10.0	(1.59)	(1.69)	
					2	.008	10.2	11.9	(1.56)	(1.71)	
3	$^{203}_{80}Hg$	HgO	-	73	0	.957	.008	.012	1.68	1.68	279
					1	.422	.002	.003	1.81	1.81	
					2	.208	.001	.001	1.89	1.80	
4	$^{181}_{72}Hf$	HfO_2	1:2	22	0	1.92	.148	.179	1.60	2.03	482
					1[b]	1.30	.068	.080	1.77	1.97	
					2	0.94	.038	.042	1.81	1.94	
5	$^{180}_{72}Hf$	HfO_2	-	60	0[b]	3.54	.065[c]	.106[c]	.148	2.05	501
					1	2.11	.037[c]	.056[c]	.193	1.99	
					2[b]	1.35	.024[c]	.034[c]	.226	1.96	
6	$^{180}_{72}Hf$	HfO_2	1:3	24	0[b]	3.73	.077[c]	.090[c]	.143	2.05	501
					1	2.19	.041[c]	.046[c]	.189	1.99	
					2[b]	1.40	.025[c]	.028[c]	.222	1.96	

(continued)

Table III.2 (continued)

Case	Parent Isotope	Chemical Form	Dilution	Effective Z	Filter Thickness w(mm)	Denominator x 10^3	$-A_{IB} \times 10^6$	$-A_B \times 10^6$	$\frac{A_\gamma}{P_{\gamma 1}} \times 10^2$	$\frac{A_{\gamma 1}}{P_{\gamma 1}} \times 10^2$	Energy of γ_1 (keV)
7	$^{198}_{79}Au$	Au_2O_3	1:30	8	0	1.65	3.49	4.21	(1.90)	(1.93)	(412)
					1	1.11	3.12	3.63	(1.89)	(1.92)	
					2	0.75	3.06	3.49	(1.85)	(1.90)	
8	$^{198}_{79}Au$	Au_2O_3	-	70	0	1.64	3.45	11.60	(1.90)	(1.93)	(412)
					1	1.11	3.11	8.97	(1.89)	(1.92)	
					2	0.75	3.06	8.11	(1.85)	(1.90)	
9	$^{159}_{64}Gd$	Gd_2O_3	1:30	7	0	.167	28.57	33.91	1.85	1.85	363
					1	.099	28.57	32.77	1.89	1.89	
					2	.060	30.34	34.27	1.86	1.86	
10	$^{159}_{64}Gd$	Gd_2O_3	-	55	0[b]	.167	28.3	79.0	1.85	1.85	363
					1[b]	.099	28.5	69.2	1.89	1.89	
					2[b]	.060	30.3	68.4	1.86	1.86	

[a] Explanation of column headings: "dilution" is by mass with carbon; "effective Z" is defined in Appendix B; "γ_1" refers in parity cases to the γ of interest, in other cases (where energies are bracketed) to the dominant γ; "A_{IB}" is the part of the asymmetry due to internal bremsstrahlung; "A_B" is total asymmetry due to bremsstrahlung = $A_{IB}+A_{EB}(\zeta = 1.5)$; "$A_\gamma/P_{\gamma 1}$" is asymmetry relative to polarization of γ_1; "$A_{\gamma 1}/P_{\gamma 1}$" is asymmetry for γ_1, alone relative to $P_{\gamma 1}$ (see Appendix A); bracketed values of A/P in last two columns are for cases where P is expected to be negligible.

[b] Values listed for completeness, but not actually used in any experiment.

[c] Bremsstrahlung from ^{181}Hf (assuming activity equal to ^{180}Hf) referred to ^{180}Hf denominator.

Table III.3 Summary of experimental results

Case	Isotope	Final Asymmetry[a] x 10^6 w = 0[b]	w = 1	w = 2	P_γ^c x 10^4
1	^{103}Ru-Rh	(controls - see text)			-
2	^{177}Lu-Hg[d]	-7.7±0.4	-10.2±0.6	-12.7±1.1	-
3	^{203}Hg-Tl	-.08±.16	-	-	
		(-.07±.16)	-	-	-.04±.10
4	^{181}Hf-Ta[d,e]	-.20±.13	-	-.10±.05	
		(.02±.13)	-	(-.06±.05)	-.031±.025
5	^{180}Hf		-5.1±1.5		
6a	^{180}Hf[e]		-3.1±2.8		-23.±6.
6b	^{180}Hf[d,e]		-3.9±2.0		
7	^{198}Au-Hg[d]	-4.4±0.2	-3.5±0.2	-3.3±0.2	-
8	^{198}Au-Hg	-10.6±0.3	-9.3±0.3	-8.6±0.3	-
9	^{159}Gd-Tb[d,e]	-38±16	-13±19	-53±17	
		(-4±16)	(+20±19)	(-19±17)	-1.±5.

[a] Unbracketed values include corrections for controls. Bracketed values also include bremsstrahlung correction.

[b] w = lead filter thickness (in mm).

[c] P_γ = polarization of γ of interest. For γ energies see column for γ_1 in Table III.2.

[d] Diluted with carbon (see Table III.1).

[e] Enriched isotope (see Table III.1).

culations for ^{177}Lu (diluted) and ^{198}Au (diluted) yields good fits to the data. Thus we have applied $\zeta = 1.5$ uniformly to the EB calculations for all cases. The bremsstrahlung is particularly important for ^{159}Gd (diluted) and ^{181}Hf (diluted), for which ^{198}Au and ^{177}Lu respectively are very good bremsstrahlung comparison cases because of similar β endpoints and allowed-shaped spectra. Note that in our diluted sources the EB contributes only about 15% to the bremsstrahlung asymmetry so that accuracy in the value of ζ is not critical. In the figures in the next two sections we display bremsstrahlung curves both for the IB component A_{IB} and the total $A_B = A_{IB} + A_{EB}(\zeta = 1.5)$.

In general we unfold the circular polarization P_{γ_1} of the γ ray of interest (denoted here as γ_1 for clarity) from the observed asymmetry A (already corrected for controls) as follows. First subtract the calculated bremsstrahlung contribution A_B (equ. A.8) from A, leaving A_γ. Then using eqn. A.9 deduce $P_{\gamma_1} = A_\gamma/(A_\gamma/P_{\gamma_1})$.

In Table III.2, the calculations are summarized. The key columns for data reduction are those for A_B and (A_γ/P_{γ_1}). In the analysis we have assigned 5% errors to these numbers.

III.3 Results for ^{180}Hf and ^{159}Tb

We discuss these cases together because both have short half-lives and expected large effects. As described in Sec. II.4 the data analysis for these cases incorporated source decay explicitly. Corrections were necessary for contaminants in both cases.

To corroborate our bremsstrahlung calculations for ^{159}Gd we have used sources of ^{198}Au. ^{180}Hf^m was unique in that no direct bremsstrahlung correction is required.

(a) $^{180}Hf^{m}$ - ^{180}Hf

The results for the three series of ^{180}Hf experiments are summarized in Table III.4. All Hf sources were irradiated for 5.5 hr in a flux of 1.2×10^{14} cm^{-2} sec^{-1} at the GETR in Pleasanton. The sources were shipped by air and the experiments commenced at t = 6 - 10 hrs. Before converting the final asymmetry to the polarization result we shall describe in detail the corrections for contaminants and control experiments.

In the $^{180}Hf^{m}$ sources, all of which were irradiated for 5.5 hr, there were contaminants of 43 day ^{181}Hf(suppressed somewhat in the enriched sources II and III). These contributed slightly to I_N and more so to I_D at $t \gg 5.5$ hr. In addition there were contaminants from the capsule requiring corrections to both I_N and I_D. Such contaminants were monitored both by γ spectroscopy of the sources and by analysis of $I_D(t)$.

Before discussing the capsule control experiments, we outline the analysis for the $^{180}Hf^{m}$ sources themselves. The "numerator" data $I_N(t)$ were fit as described in Sec. II.4 to determine initial amplitudes $I_N^1(0)$ and $I_N^2(0)$ corresponding to half-lives T_1 = 5.5 hr ($^{180}Hf^{m}$) and T_2= 43 day. The "denominator" data $I_D(t)$ were fit for three components $I_D^1(0)$, $I_D^2(0)$ and $I_D^3(0)$ with T_1 = 5.5 hr, T_2 = 43 day and T_3 = 40 hr. The value of T_3 was selected by χ^2-tests to accomodate small amounts of capsule contaminants with decay rates in this intermediate range. Let us distinguish the values $I_N^1(0)$ and $I_D^1(0)$ thus obtained as $I_N^1(0)_{Hf+cap}$ and $I_D^1(0)_{Hf+cap}$, where "cap" is short for capsule.

Two control experiments were performed with capsules (irradiated

Table III.4. Results for $^{180}Hf^{m}$ experiments. [a]

Series	Source material isotopic composition [b] % ^{179}Hf	% ^{180}Hf	Chemical form	Mass(g) of Hf	Number of experiments	Chi square	Raw asymmetry x 10^6	Final asymmetry [c] x 10^6
I	14	35	Hf Rod	50	1	2.1	-3.5 ± 1.4	-5.1 ± 1.5
			HfO_2 Powder	15	5			
II	75	14	HfO_2 Powder	0.75	5 [d]	4.6	-9.6 ± 1.8	-3.1 ± 2.8 [e]
III	58	30	HfO_2 Powder [f]	1.0	3 [d]	4.8	-2.6 ± 1.8	-3.9 ± 2.0
					(Mean asymmetry) x 10^6			-4.4 ± 1.1
					(Asymmetry referred to 501 keV γ) x 10^6			-46 ± 11

[a] All measurements were performed with a 1 mm lead filter around the source.

[b] Isotopic abundance prior to irradiation. Series I used natural abundance material; II and III used enriched material in order to suppress ^{181}Hf.

[c] Corrected for ^{103}Ru control $A_{Ru} = (-0.20 \pm 0.03) \times 10^{-6}$ and for capsule control $A_{cap} \sim (1.6 \pm 0.5) \times 10^{-6}$.

[d] Successive irradiations of one sample.

[e] Corrected for effects of ^{24}Na contaminant present in this sample alone: $A_{Na} = (-8.1 \pm 2.0) \times 10^{-6}$.

[f] Diluted 1:3 by mass with carbon powder.

5.5 hr) containing no Hf powder. The data were fit exactly as above yielding in particular values $I_N^1(0)_{cap}$ and $I_D^1(0)_{cap}$. The latter was subtracted from $I_D^1(0)_{Hf+cap}$ yielding $I_D^1(0)_{Hf}$ for each case; this correction amounted to about 10% only. At this point we define $A_{raw} = I_N^1(0)_{Hf+cap}/I_D^1(0)_{Hf}$. Values for this raw asymmetry are given in the second last column of Table III.4 (The value for series II contains yet a large Na contaminant which will be discussed below). Finally we subtract from A_{raw} the values $A_{cap} = I_N^1(0)_{cap}/I_D^1(0)_{Hf}$ yielding A_{final}. Equivalently $A_{final} = I_N^1(0)_{Hf}/I_D^1(0)_{Hf}$ where $I_N^1(0)_{Hf} = I_N^1(0)_{Hf+cap} - I_N^1(0)_{cap}$. Values of A_{final} are given in the last column of Table III.4. We present the results in this way to emphasize the original concern that perhaps $I_N^1(0)_{cap}$ might have been producing the non-zero effect in A_{raw}. But in fact we found A_{cap} to have <u>opposite</u> sign thus requiring actually an increase in $|A_{raw}|$ to obtain A_{final}. Referred to an average $I_D^1(0)_{Hf}$ the value of A_{cap} was $\sim (+1.6 \pm 0.5) \times 10^{-6}$.

The presence of the large Na contaminant in the enriched material of series II was established quantitatively by γ spectroscopy. The relative γ intensities indicated the ratio of initial activities of ^{24}Na to $^{180}Hf^m$ to be $(.25 \pm .06)$ corresponding to about 27 mg Na. We calculated that the ^{24}Na bremsstrahlung contribution from the 1.39 MeV endpoint β decay with 15 hr half-life would produce an apparent asymmetry (referred to $I_D^1(0)_{Hf}$) of $A_{Na} = (-8.1 \pm 2.0) \times 10^{-6}$. The corrected value A_{final} (series II) $= (-3.1 \pm 2.8) \times 10^{-6}$ is consistent with the other results, but carries less statistical weight because of the enlarged error.

The purity of the enriched powder in <u>series III</u> was checked doubly

by chemical analysis (flame photometry) and by activation analysis and found to contain < 1 ppm of Na. Furthermore γ spectroscopy of the sources in all three series established the absence of any other appreciable contaminants.

We considered also the possibility, albeit remote, that the observed asymmetry might be due to bremsstrahlung from 4.6 hr ^{179}Lu produced by ^{179}Hf(n,p)^{179}Lu in the reactor fast flux. It was difficult to reject this possibility by γ spectroscopy alone since the sole 217 keV γ from ^{179}Lu decay would be hidden below the 215.3 keV γ peak of ^{180}Hf. A control experiment with a Hf source irradiated within a cadmium shell (to absorb thermal neutrons and thereby suppress ^{180}Hf) was performed. The effective asymmetry for this $I_N^1(0)_{Hf(Cd)}$ relative to the usual $I_D^1(0)_{Hf}$ was $A_{Hf(Cd)} = (+1.4 \pm 2.3) \times 10^{-6}$, in contrast to $A_{Hf} = (-4.4 \pm 1.1) \times 10^{-6}$. This result together with γ spectra of the Hf(Cd) source indicated the absence of ^{179}Lu.

The residual asymmetry of the system was determined with the fast 497 keV γ of ^{103}Rh following β-decay of ^{103}Ru. After a small bremsstrahlung correction we found the control asymmetry $A_{Ru} = (-0.20 \pm 0.03) \times 10^{-6}$. The results have been corrected for this small background asymmetry.

The mean final asymmetry $(-4.4 \pm 1.1) \times 10^{-6}$ (shown in Fig.III.1(a) below the decay scheme) corresponds to a polarization of the 501 keV γ of ^{180}Hf given by

$$P_\gamma = (-2.3 \pm 0.6) \times 10^{-3}$$

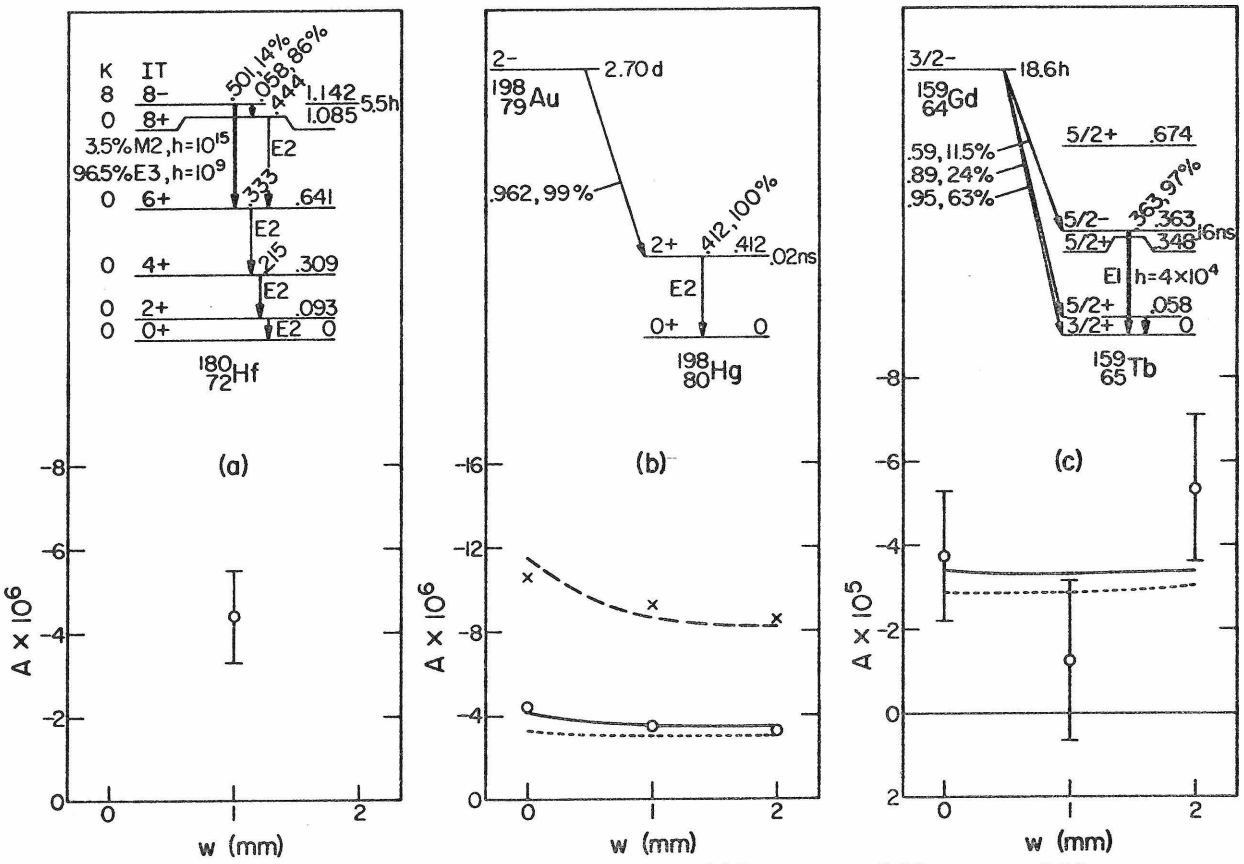

Fig. III.1 Asymmetry A vs lead filter thickness w for (a) $^{180}Hf^{m}$ (b) ^{198}Au (c) ^{159}Gd. In (b) and (c) the circles and solid curves are respectively the experiments and total (IB + EB) β bremsstrahlung calculations for sources diluted with carbon. The dotted curves show the IB component alone. In (b) the crosses and dashed curve are the experiments and IB + EB calculations for the undiluted source. The decay schemes shown in (b) and (c) are partial. The hindrance factors h are relative to the Weisskopf estimate. In (b) the errors are about the size of the data points. The bremsstrahlung curves have 5% errors. The asymmetry in (a) is attributed to circular polarization of the 501 keV γ. In (c) any net deviation of the data from the solid curve would be attributed to circular polarization of the 363 keV γ of ^{159}Tb.

(b) ^{198}Au - ^{198}Hg

We chose ^{198}Au specifically to check the bremsstrahlung asymmetry calculations for ^{159}Gd, because of their similar β endpoints and γ energies. (Compare decay schemes in Fig. III.1(b) and (c).) To this end we prepared a source of 100 mg Au_2O_3 diluted with 3 g C powder, the same composition as the Gd_2O_3 source.

In addition we used an undiluted Au_2O_3 source to determine the parameter ζ in our EB calculations (see Sec. B.1). In Fig. B.1(a) we show the calculated IB and EB ($\zeta = 1$) spectra and polarizations for the 962 keV β endpoint of ^{198}Au for both diluted and undiluted sources.

Using these results we then calculated (Appendix A) the respective asymmetries (referred to the 412 keV γ) A_{IB} and $A_{EB(\zeta = 1)}$. Then we evaluated ζ by comparison to the experiments on the undiluted source: $A^{(w)}_{expt} \sim A^{(w)}_{IB} + A^{(w)}_{EB(\zeta = 1)}/\zeta$, with w = 0, 1, 2 mm. This gave $\zeta = 1.5$. The fit is shown in the dashed curve and crosses in Fig.III.1(b).

Using $\zeta = 1.5$ for the <u>undiluted</u> source we find very good agreement between calculations and experiment. This gives confidence in similar calculations for ^{159}Gd.

(c) ^{159}Gd - ^{159}Tb

The one Gd source (irradiated three times for 18 hr) was composed of 100 mg Gd_2O_3 enriched to 92% in ^{158}Gd mixed with 3 g C powder. The dilution served two purposes (a) to suppress EB and (b) to provide a large surface-to-volume ratio for the Gd powder to minimize self-shielding effects by ^{155}Gd and ^{157}Gd which have resonances in the thermal neutron range. The enrichment suppressed ^{155}Gd and ^{157}Gd relative to

^{158}Gd.

The "numerator" data $I_N(t)$ were fit with only one component $I_N(0)$ with half-life T = 18.6 h for ^{159}Gd. Just as with ^{180}Hf we ran a capsule control (here irradiated for 18 hr like the Gd source). The contribution to $I_D(t)$ was considerable here because of the lower γ intensity from ^{159}Gd. Therefore we subtracted graphically the data $I_D(t)_{cap}$ from $I_D(t)_{Gd+cap}$. The resultant $I_D(t)_{Gd}$ indeed fit well to 18.6 h decay, yielding $I_D(0)_{Gd}$. The capsule asymmetry here was effectively $A_{cap} = I_N(0)_{cap}/I_D(0)_{Gd} \approx (-0.3 \pm 1.6) \times 10^{-5}$. (The fact that this differs from A_{cap} for $^{180}Hf^m$ is due to (i) different irradiation times (ii) different half-lives in the data analysis and (iii) different denominators $I_D^1(0)_{Hf}$ and $I_D(0)_{Gd}$.)

The results including this correction are displayed in Fig. III.1(c) and Table III.3. Subtracting the bremsstrahlung calculations from the data points we obtain the three bracketed values for Gd in Table III.3. The mean asymmetry for the 363 keV γ of ^{159}Tb is then $A = (-2 \pm 10) \times 10^{-6}$ corresponding to a circular polarization

$$P_\gamma = (-1 \pm 5) \times 10^{-4}$$

III.4 Results for ^{203}Tl and ^{181}Ta

We group these cases together because of their common properties of long half-life and small effect. Relatively large corrections are required here for residual asymmetries observed in Ru controls.

In connection with the ^{181}Hf bremsstrahlung, we present results for the ^{177}Lu comparison case, which has a comparable β endpoint and

spectrum shape. For ^{203}Hg with lower endpoint the bremsstrahlung is less important.

Capsule contaminants were negligible for these long-lived cases with high activities.

(a) ^{203}Hg - ^{203}Tl

For these measurements the polarimeter was in an intermediate assembly (see Sec. II.6(i)) for which Ru controls before and after gave a background asymmetry:

$$A_{Ru} = (+ 0.27 \pm 0.07) \times 10^{-6} \quad ,$$

after bremsstrahlung corrections. This control pertains to a γ energy of 497 keV, whereas in ^{203}Tl the γ energy is only 279 keV. Depending on what was really causing the background, the control for 279 keV could be the same or perhaps less. Assuming that in the energy range below 500 keV, the behavior of the background is intermediate between being constant and being in proportion to energy, we project the control to 279 keV as

$$A_{279} = (+ 0.20 \pm 0.15) \times 10^{-6}$$

We have increased the error conservatively to be compatible with either hypothetical energy dependence.

All ^{203}Hg runs were performed with no lead filter (w = 0), since the 279 keV γ would have been appreciably absorbed and since the bremsstrahlung was minor. In the earlier runs there was a fast decaying ^{198}Au component in I_D and I_N. This was produced by the peculiar chain: $^{196}Hg(n,\gamma)$ ^{197}Hg(E.C.β decay) $^{197}Au(n,\gamma)$ ^{198}Au. In the analysis we readily separated the ^{203}Hg component from this short-lived contaminant.

The raw asymmetry for ^{203}Hg was $A_{raw} = (+ .12 \pm .06) \times 10^{-6}$. Subtracting the control A_{279} we obtain $A_{Hg} = (-.08 \pm .16) \times 10^{-6}$. For $w = 0$, $A_B = -.01 \times 10^{-6}$ (5% error). The value of A_{Hg} and the curve A_B are shown together with the decay scheme in Fig. III.2(a). Subtracting we obtain $A_{Tl} = (-.07 \pm .16) \times 10^{-6}$. Finally, we obtain the circular polarization of the 279 keV γ of ^{203}Tl

$$P_\gamma = (-4 \pm 10) \times 10^{-6}$$

(b) ^{177}Lu

^{177}Lu was chosen to check the efficiency and bremsstrahlung calculations, in particular for ^{181}Hf. The β decays for ^{177}Lu and ^{181}Hf may be compared by inspection of the respective decay schemes in Fig. III.2(b) and (c). Curves for the spectra and polarization of IB and EB($\zeta = 1$) are given in Appendix B for the 497 keV β branch of ^{177}Lu.

The calculated and measured asymmetry results ($\zeta = 1.5$) are shown in Fig. III.2(b) and Tables III.2 and III.3. The good agreement between calculation and experiment supports the bremsstrahlung calculations used for ^{181}Hf.

(c) ^{181}Hf - ^{181}Ta

A portion of the ^{181}Hf data was taken with the magnet polarity switch (Fig. II.3) reversed; in this case the sign of A was opposite to that of the LIA output. In this section we use a superscript (+) or (-) to denote the normal or reversed polarity. In addition we include the filter thickness w in the superscript, when relevant.

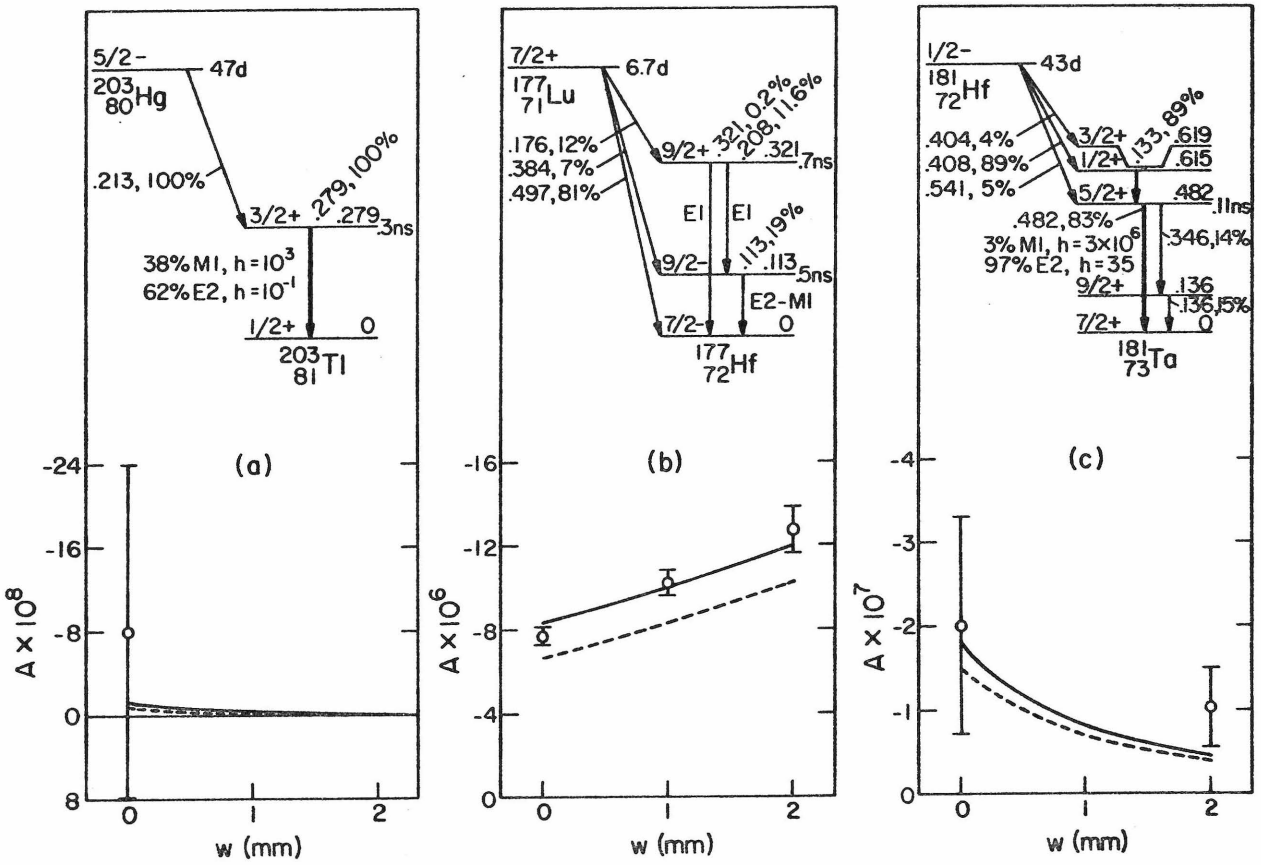

Fig. III.2 Asymmetry A vs lead filter thickness w for (a) ^{203}Hg (b) ^{177}Lu and (c) ^{181}Hf. For explanation of symbols see caption of Fig. III.1

The raw Hf data gave

$$A^{(0+)}_{Hf,raw} = (-.406 \pm .126) \times 10^{-6}$$

$$A^{(2+)}_{Hf,raw} = (-.311 \pm .047) \times 10^{-6}$$

$$A^{(2-)}_{Hf,raw} = (-.371 \pm .070) \times 10^{-6}$$

For the corresponding ^{103}Ru controls we found after bremsstrahlung correction

$$A^{(+)}_{Ru} = (-.205 \pm .028) \times 10^{-6}$$

$$A^{(-)}_{Ru} = (-.277 \pm .058) \times 10^{-6}$$

The 497 keV γ from ^{103}Ru is a very suitable control for the 482 keV γ from ^{181}Hf. Thus we subtract the controls directly from the data obtaining

$$A^{(0)}_{Hf} = (-.201 \pm .129) \times 10^{-6}$$

$$A^{(2)}_{Hf} = (-.103 \pm .047) \times 10^{-6}$$

where we have combined the w = 2 results.

These values as well as bremsstrahlung curves (see also Table III.2) are plotted in Fig. III.2(c). Subtracting bremsstrahlung we obtain

$$A^{(0)}_{Ta} = (-.022 \pm .129) \times 10^{-6}$$

$$A^{(2)}_{Ta} = (-.060 \pm .047) \times 10^{-6}$$

Using values of (A_γ/P_{γ_1}) in Table III.2 we find polarizations respectively

$$P_\gamma = (-1.4 \pm 8.1) \times 10^{-6}$$

$$P_\gamma = (-3.3 \pm 2.6) \times 10^{-6}$$

The final results from the polarization of the 482 keV γ in ^{181}Ta is

$$P_\gamma = (-3.1 \pm 2.5) \times 10^{-6}$$

IV. DISCUSSION

IV.1 Introduction

The results of Chapter III are now compared to values from other experiments and to theoretical predictions. For reference we present in Table IV.1 a summary of experiments measuring P_γ from unoriented nuclei.[5,6,22-31] We include only the four nuclei studied herein.

IV.2 ^{180}Hf 501 keV γ

This transition has the largest P_γ yet observed in (non-leptonic) parity experiments. Our value $P_\gamma = (-2.3 \pm 0.6) \times 10^{-3}$ is in good agreement with the value reported by Jenschke and Bock[22] $P_\gamma = (-2.8 \pm 0.45) \times 10^{-3}$.

The decay scheme is shown in Fig. III.1(a). The 501 keV γ between the 1142 keV 8^- (K = 8) isomeric state and the 641 keV 6^+ (K = 0) state has multipolarity M2 - E3 - $(\widetilde{E2})$ with regular mixing ratio $\delta^2 \approx 30$. Transitions from the isomeric state to the ground-state rotational band (K = 0) are strongly hindered by virtue of their high K forbiddenness. (See hindrances h in Fig. III.1(a)).

The unusually large polarization observed here is due presumably to two main features (a) the irregular multipole, being E2, is strongly enhanced (factor $(100)^{1/2} = 10$ for the amplitudes within a single-particle model) compared to the regular M2 and (b) in perturbation theory, the closeness of the 8^- (K = 8) and 8^+ (K = 0) levels (58 keV) enhances the admixture by the PNC force.

However since V^{PNC} itself (lacking collective character) would not mix states of different K, we must invoke a collective mechanism, such

Table IV.1. Comparison with other experimental results.

Nucleus	γ-Ray Energy (keV)	$P_\gamma \times 10^4$	Authors
^{180}Hf	501	-23 ± 6	this work
		-28 ± 4.5	Jenschke and Bock[22]
^{159}Tb	363	-1 ± 5	this work
^{203}Tl	279	-.04 ± .10	this work
		+.016 ± .05	Vanderleeden, Boehm & Lipson[23]
		-.2 ± .3	Boehm and Kankeleit[24]
		.0 ± .1	Kankeleit and Kuphal[25]
		-.30 ± .18	De Saintignon and Chabre[26]
		-.014 ± .039	...Mean (χ^2_ν=3.36, ν= 4, $P(\chi^2>\chi^2_\nu)$ = .50)
^{181}Ta	482	-.031 ± .025	this work
		-.06 ± .01	Lobashov et al[5]
		-.039 ± .012	Vanderleeden and Boehm[6]
		-.041 ± .013	Bock and Jenschke[27]
		-.04 ± .08	Kankeleit and Kuphal[25]
		-.1 ± .4	Boehm and Kankeleit[24]
		+.7 ± .7	van Rooijen et al[28]
		-.9 ± .6	Cruse and Hamilton[29]
		-.21 ± .11	De Saintignon et al[30]
		-.28 ± .06	Bodenstedt et al[31]
		-.051 ± .006	...Mean (χ^2_ν= 22.9, ν = 9, $P(\chi^2>\chi^2_\nu)$ = .007)

as Coriolis (rotation-particle) coupling. From this point of view we may represent the 1142 keV state as

$$|\psi_{1142}\rangle = |8^- K=8\rangle + \frac{\langle 8^+ K=0|H^{(8)}_{Coriolis}|8^+ K=8\rangle \langle 8^+ K=8|V^{PNC}|8^- K=8\rangle}{\Delta E}|8^+ K=0\rangle$$

where the first "matrix element" is actually an abbreviation for Coriolis coupling in eighth order perturbation theory, since the Coriolis operator $\frac{-\hbar^2}{2I}(J_+ j_- + J_- j_+)$ can change K by only one unit in each order. The value of ΔE is -58 keV. The $\widetilde{E2}$ transition proceeds unhindered between the $|8^+ K = 0\rangle$ admixture and the $|6^+ K = 0\rangle$ state.

Vogel[32] has estimated P_γ using such Coriolis mixing with strength in each order given roughly by

$$\frac{\hbar^2}{2I}\frac{((J-K)(J+K+1))^{1/2}\langle K+1|j_+|K\rangle}{E_{K+1}-E_K} \approx (15\text{ keV})\ \frac{(7)\ (3)}{(2\text{ MeV})} = .15$$

compatible with regular multipole transition ratios from the isomeric state. This leads to his estimate $|P_\gamma| \lesssim 2 \times 10^{-3}$, which is in agreement with our observation.

A number of related experiments are possible in ^{180}Hf. The 58 keV transition between the 8^- and 8^+ states should show a comparable polarization. It is more difficult to measure because of its low energy. The present limit for this transition is $|P_\gamma| < 5\%$.[33] Another possibility is to search for anomalous internal-conversion coefficients for this γ; however the interpretation is complicated by penetration effects.[34] Finally for the 501 keV γ it would be desirable to seek an E3($\widetilde{E2}$) interference (not diluted by $\delta = 0.2$ as is the M2($\widetilde{E2}$)

interference observable in P_γ) in an angular distribution experiment from oriented nuclei. Continued experimental and theoretical investigations of this outstanding nucleus ^{180}Hf would be highly desirable.

IV.3 ^{159}Tb 363 keV γ

After the successful observation on ^{180}Hf we were led to consider ^{159}Tb which has similarly an opposite parity state very near the initial state. The partial decay scheme is shown in Fig. III.1(c). The E1 transition between the 363 keV 5/2 $5/2^-$ [532] state (notation $J\ K^\pi\ [N\ n_z \Lambda]$ in Nilsson scheme) and the ground state 3/2 $3/2^+$ [411] has hindrance $h = 4 \times 10^4$ relative to the Weisskopf estimate. The neighboring 348 keV state has quantum numbers 5/2 $5/2^+$ [413]. Admixture of this into the 363 keV state would permit an $\widetilde{M1}$ transition as well as $\widetilde{E2}$. All three multipolarities E1, $\widetilde{M1}$, $\widetilde{E2}$ are hindered by asymptotic selection rules.

Using Nilsson-model (single particle in deformed potential) wave functions Vogel[32] has estimated P_γ for the 363 keV γ. He finds that indeed the 348 keV state should dominate the parity mixing (note the two other known $5/2^+$ states available). Furthermore the $\widetilde{M1}$ reduced matrix element should exceed the $\widetilde{E2}$ (see below). Vogel's estimate is $|P_\gamma| \lesssim 4 \times 10^{-4}$ in agreement with our measurement $P_\gamma = (-1 \pm 5) \times 10^{-4}$.

In an experiment with nuclei polarized by cryogenic techniques, Pratt et al[35] have reported an asymmetry $1 + A_1\ P_1(\cos\theta)$ with $A_1 = (+4.5 \pm 3.0) \times 10^{-3}$ in the angular distribution of the 363 keV γ. In order to compare their results to ours we have evaluated for this

transition the general expressions for A_1 and P_γ given by Blin-Stoyle [11], obtaining

$$A_1 = 2B_1(5/2)\left(F_1(11\ \tfrac{3}{2}\ \tfrac{5}{2})\frac{\langle\tilde{M1}\rangle}{\langle E1\rangle} + F_1\ (12\ \tfrac{3}{2}\ \tfrac{5}{2})\ \frac{\langle\tilde{E2}\rangle}{\langle E1\rangle}\right)$$

$$= 2 \times 1.464\left(-1.025\ \frac{\langle\tilde{M1}\rangle}{\langle E1\rangle} + 0.520\ \ \frac{\langle\tilde{E2}\rangle}{\langle E1\rangle}\right)$$

$$P_\gamma = 2\ \frac{\langle\tilde{M1}\rangle}{\langle E1\rangle}$$

where $\langle E1\rangle, \langle\tilde{M1}\rangle, \langle\tilde{E2}\rangle$ denote reduced matrix elements. If we assume $\langle\tilde{E2}\rangle \ll 2\langle\tilde{M1}\rangle$ then

$$A_1 = -1.50\ P_\gamma$$

and our result would correspond to

$$A_1 = (-0.2 \pm 0.8) \times 10^{-3}\ .$$

Thus unless somehow $\langle\tilde{E2}\rangle \gg 2\langle\tilde{M1}\rangle$ (i.e. mixing ratio for 348 keV transition $\delta^2 \gg 4$), the parity admixtures in the 363 keV state seem considerably lower than indicated by the experiment of Pratt et al.[35]

IV. 4 ^{203}Tl 279 keV γ

The partial decay scheme for ^{203}Tl is shown in Fig. III.2(a). The 279 keV γ has regular multipolarity M1 - E2 ($\delta^2 \approx 1.6$) and irregular multipolarity $\tilde{E1}$. The single-particle (proton hole) assignments for

the initial and final states are $(2d_{3/2})^{-1}$ and $(3s_{1/2})^{-1}$ respectively. Thus the regular M1 is hindered ($h = 10^3$) by ℓ-forbiddenness. Szymanski[36] has estimated for this transition $P_\gamma = (-0.9 \pm 0.3) \times 10^{-4}$.

In Table IV.1 we compare our result $P_\gamma = (-.04 \pm .10) \times 10^{-4}$ to four other experimental results. The overall trend indicates that the estimate above is too high by an order of magnitude at least. Thus parity admixtures (if any) in ^{203}Tl are lower than predicted and lower than can be resolved by experiments to date.

IV.5 ^{181}Ta 482 keV γ

This transition has been by far the most popular for such studies (see Table IV.1), although in retrospect the enthusiasm is somewhat dubious. The decay scheme is shown in Fig. III.2(c). The transition of interest proceeds from the 482 keV 5/2 $5/2^+$ [402] state to the 7/2 $7/2^+$ [404] ground state. The regular M1 is strongly hindered ($h = 3 \times 10^6$) and the E2 slightly hindered ($h = 35$); the M1-E2 mixing ratio is $\delta^2 \sim 30$. One hopes that the relative enhancement of $\widetilde{E1}$ may lead to a large P_γ here.

Early estimates by Michel[37] and Wahlborn[38] using a single particle force (including ρ exchange potential V_ρ but not V_π) of the form $\vec{\sigma} \cdot \vec{p}$ and Nilsson wave functions gave $|P_\gamma| = 1 \times 10^{-4}$ and $P_\gamma = (-0.6 \pm 0.3) \times 10^{-4}$ respectively. Maqueda and Blin-Stoyle[39] using a <u>static</u> two-body potential of the form $\vec{r}_{12} \cdot \vec{\sigma}_1 \times \vec{\sigma}_2$ predicted $P_\gamma = -0.7 \times 10^{-4}$. More recently McKellar[40] considered in more detail the effects of two-body correlations (due to N-N hard core). With the inclusion of V_ρ and V_π (the latter contributing $\sim 20\%$), McKellar

estimated $P_\gamma = (-0.2 \pm 0.1) \times 10^{-4}$. Vinh Mau and Bruneau[41] evaluated V_π (claiming V_ρ to be suppressed by a factor of ~ 8) and obtained $P_\gamma = -0.008 \times 10^{-4}$ much smaller than previous estimates. Finally Gari et al[42] reconsidering short-range correlations predict (with V_ρ and V_π) $P_\gamma \approx + 0.0003 \times 10^{-4}$. Thus in eight years theoretical estimates for ^{181}Ta have fallen by over three orders of magnitude. Clearly the theoretical question is still open.

In Table IV.1 we note the excellent agreement among the top four ^{181}Ta experiments, all of which achieved small statistical errors by means of integral detection techniques. The mean of these four studies is the small but finite value $P_\gamma = (-.048 \pm .006) \times 10^{-4}$ with $\chi^2_\nu = 2.75$, $\nu = 3$, $P(\chi^2 > \chi^2_\nu) = .45$. Most theoretical estimates are either too high or too low compared to this result. The last three experiments listed (which used singles-counting techniques) seem to claim a much larger effect despite their lower precision. The discrepancy is irreconcilable without detailed inspection of systematic errors in these experiments. Our value $P_\gamma = (-.031 \pm .025) \times 10^{-4}$, while not the most precise to date, does support the camp claiming a small finite value. The mean of all ten experiments is found (with a rather poor χ^2 probability) to be $P_\gamma = (-.051 \pm .006) \times 10^{-4}$. (The "external error" is $.010 \times 10^{-4}$.)

IV. 6 Conclusion

Our result in ^{180}Hf has established the presence of a PNC force, whereas in ^{159}Tb we have reduced the upper limit of parity mixing suggested by a related experiment elsewhere. In ^{203}Tl we have confirmed

that the parity admixtures are lower than originally predicted. Finally in ^{181}Ta we support the presence of a small but finite PNC effect. We hope that the results herein particularly the ^{180}Hf result will stimulate further theoretical study both in nuclear structure considerations, such as short range correlations, and in the structure of the non-leptonic weak-interactions.

APPENDIX A

POLARIMETER EFFICIENCY CALCULATIONS

A.1 Relation Between Asymmetry and Polarization

We first formulate the dependence of the detector current I and asymmetry A on the initial photon spectrum $\frac{dN}{dk}$ and circular polarization P(k). For the present we neglect source decay which contributes an overall exponential factor to I and we assume the magnetization follows an ideal square wave (the effects of waveform distortions are discussed in Appendix C). Let $A_s(k)$ represent the absorption of photons in the source material and container such that $A_s(k)\frac{dN}{dk}$ is the spectrum of photons leaving the source region.

We decompose $\frac{dN}{dk}$ into bremsstrahlung quanta $\frac{dN_B}{dk}$ and gamma rays N_i of energy k_i

$$\frac{dN}{dk} = \frac{dN_B}{dk} + \sum_i N_i \, \delta\,(k-k_i) \tag{A.1}$$

and P(k) into components $P_B(k)$ for bremsstrahlung and P_i for gammas.

$$P(k)\,\frac{dN}{dk} = \frac{dN_R}{dk} - \frac{dN_L}{dk} = P_B(k)\,\frac{dN_B}{dk} + \sum_i P_i N_i \delta(k-k_i) \tag{A.2}$$

where $\frac{dN_R}{dk}\left(\frac{dN_L}{dk}\right)$ refers to right(left) handed circularly polarized photons. Finally we define the polarimeter intensity detection function

$$D(k) = \frac{\langle k_D \rangle}{k} \qquad \text{for} \quad P(k) = +1$$

where k is again the energy of the photon leaving the source and $\langle k_D \rangle$ is the expectation of the energy deposited in the detector by the resultant scattered photon. It is convenient to expand D(k) in a power series in f(t), where f(t) denotes the fraction of polarized electrons (positive in the forward direction):

$$D(k) = D_0(k) + D_1(k)f + D_2(k)f^2 + O(f^3) \tag{A.3}$$

The terms $O(f^3)$ can be neglected since both D_n and f^n fall off rapidly with n.

If we correspondingly decompose the detector current as

$$I(t) = I_0 + I_1(t) + I_2(t) \tag{A.4}$$

we find that

$$\begin{aligned} I_0 &= C \int D_0(k)\, A_s(k) k \frac{dN}{dk}\, dk \\ I_1(t) &= C\, f(t) \int D_1(k)\, A_s(k)\, P(k)\, k \frac{dN}{dk}\, dk \\ I_2(t) &= C\, f^2(t) \int D_2(k)\, A_s(k)\, k \frac{dN}{dk}\, dk \end{aligned} \tag{A.5}$$

where C is a constant depending on the detector's conversion of the photon energy to current. Note that P(k) appears linearly only in terms odd in f(t), here $I_1(t)$. We now define the asymmetry

$$A = \frac{I\{f = -f_0\} - I\{f = +f_0\}}{I\{f = -f_0\} + I\{f = +f_0\}}$$

With this sign convention A will have the same sign as P, since

$\frac{D_1(k)}{D_0(k)} < 0$ in our geometry.

Then

$$A = -f_0 \frac{\int D_1(k)\ A_s(k)\ P(k)\ k\ \frac{dN}{dk}\ dk}{\int D_0(k)\ A_s(k)\ k\frac{dN}{dk}\ dk} \tag{A.6}$$

$$= -f_0 \frac{\Sigma\ D_1(k_i)\ A_s(k_i)\ P_i\ k_i\ N_i + \int\ D_1(k)\ A_s(k)\ P_B(k) k\ \frac{dN_B}{dk}\ dk}{\Sigma\ D_0(k_i)\ A_s(k_i)\ k_i\ N_i \quad + \int\ D_0(k)\ A_s(k)\ k\ \frac{dN_B}{dk}\ dk} \tag{A.7}$$

where we have neglected the term of order f^2 in the denominator. The bremsstrahlung intensity term in the denominator is generally orders of magnitude below the gamma intensity. In most cases of interest only one gamma transition (denoted by γ_1) will have appreciable net polarization P_{γ_1}. We then write

$$A = A_B + A_\gamma$$

with

$$A_B = -\ f_0 \frac{\int\ D_1(k)\ A_s(k)\ P_B(k)\ k\ \frac{dN_B}{dk}\ dk}{\{DENOM\}} \tag{A.8}$$

and

$$A_\gamma = -\ f_0\ P_{\gamma_1} \quad \frac{D_1(k_{\gamma_1})\ k_{\gamma_1}\ N_{\gamma_1}}{\{DENOM\}} \tag{A.9}$$

where {DENOM} is the denominator of (A.7).

If the transition γ_1 is all that is observed then

$$A = -\ f_0\ P_{\gamma_1}\ \frac{D_1\ (k_{\gamma_1})}{D_0\ (k_{\gamma_1})}$$

For this special case (more relevant to singles counting experiments) the expression $-f_0 D_1(k_{\gamma_1})/D_0(k_{\gamma_1})$ is called the "efficiency" for detecting the polarization of a photon of energy k_{γ_1}. For example if k_{γ_1} = 500 keV the efficiency is roughly 0.3 x 0.067 = 0.02. Thus the observed asymmetry would be only 2% of the net polarization P_{γ_1}.

A.2 Monte Carlo Calculation of $D_n(k)$

The actual polarimeter is shown in Fig. II.1. The polarimeter treated by the program (Fig. A.1(a)) has the following simplifications: the magnet is a uniformly magnetized annular cylinder; the source is a point; the detector is an opaque sphere; the plug is opaque; the magnet inner surface with $z < B$ is opaque as is the magnet volume $z < A$. Although the figures show the cylindrical lead filter with thickness 1 mm, we have run experiments and the program with 0 mm and 2 mm as well. We have used a modified version of the program for another polarimeter [6] which has disc shaped lead between source and plug filters. Despite the different dimensions, results for both systems are quite similar.

To illustrate the procedure let us follow the trajectory indicated in Fig. A.1(a). Beginning at the source (1) in a preassigned direction we determine an intersection with the filter and compute the distance through the filter in that direction. Then with reference to the entry point we generate a random distance for an interaction (2), specifically Compton scattering or photoelectric absorption. If the photon has not escaped we reduce the statistical weight (see below) to allow for absorption and then generate a Compton scattering direction. This pro-

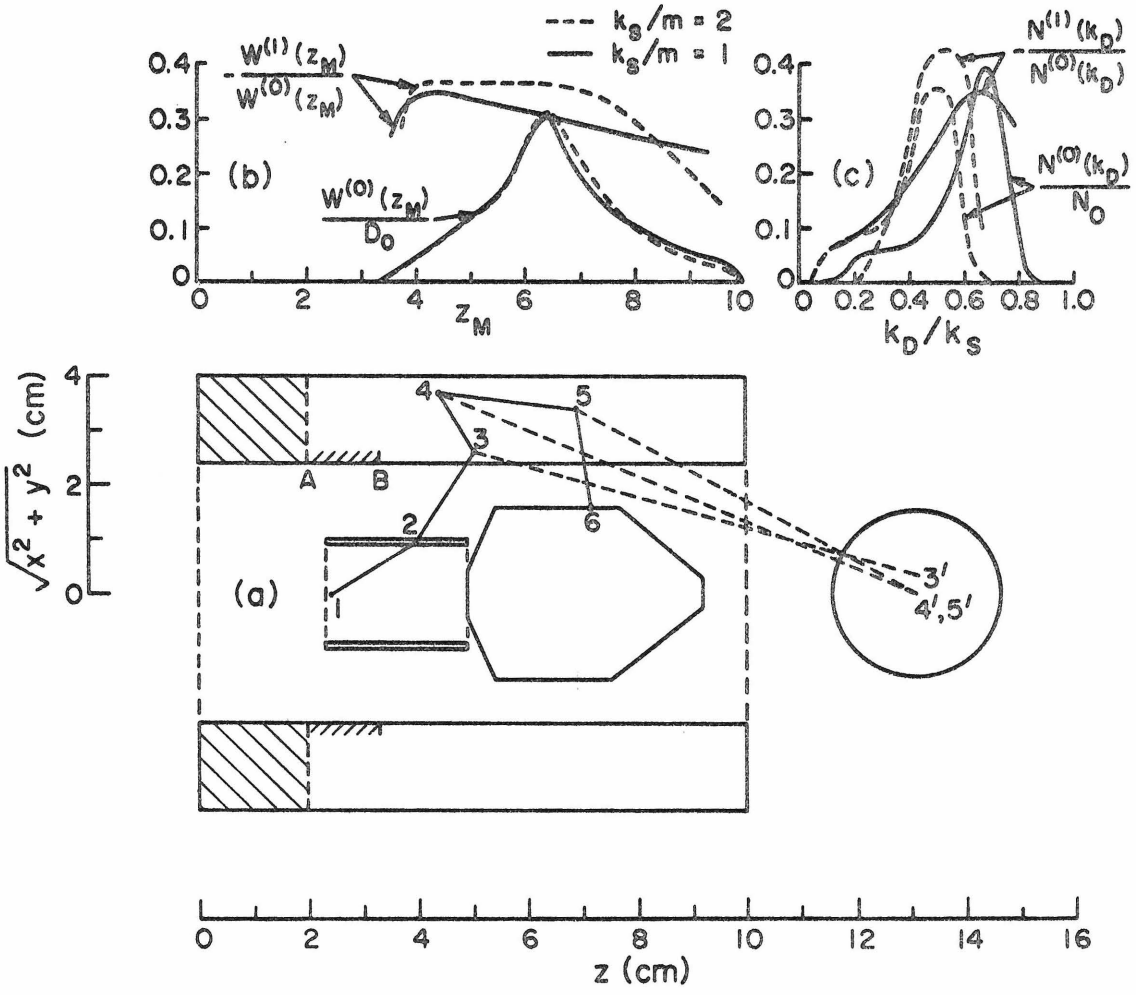

Fig. A.1 (a) Simplified polarimeter geometry used in Monte Carlo program. (b) Efficiency and distribution of detected energy vs magnet coordinate z_M. (c) Efficiency and spectra for final energy k_D. See text.

cess is repeated until the photon escapes or exceeds a scattering order limit for the material, here lead. If the escape is in a direction that misses the plug and intersects the magnet at $z > B$, the photon proceeds in a similar fashion to that with the filter, with one exception: upon determining a scattering position (3) we immediately force a scatter to the center of the unobscured region of the detector (3') and record the final probability in a two dimensional histogram for the last magnet z-coordinate z_M and the final detected energy k_D. Then with reduced weight we continue the random scatterings. The termination (not including forced branches to the detector) of each initial photon is tallied in eleven categories including: escape from the system, entry to forbidden zones, exceeding scattering order limits, hitting the plug (as shown at (6) in the example), having an energy below some cutoff and "accidental" detection.

To carry the photon polarization and intensity through successive Compton scatters in lead and magnetic iron we take advantage of an elegant matrix formalism using the four-component Stokes vector $\underline{S}$ and 4 x 4 transformation matrix $\underline{\underline{T}}$[43]. In this formalism which follows from the density matrix[44] representation, the photon polarization is treated statistically in the sense of an ensemble average, although for individual photons the polarization is quantized (viz circular polarization $P_c = \pm 1$). In the same spirit we will treat the electron polarization $\vec{s}$ statistically putting $\vec{s} \equiv \vec{0}$ (null vector) in lead and $\vec{s} = f\hat{e}_z$ in iron for each electron.

In the Stokes vector the first component $S_1 \equiv I$ is the intensity. If we introduce a "normalized Stokes vector" $\underline{\tilde{S}} = \underline{S}/I$, then $\tilde{S}_2$, $\tilde{S}_3$ are

linear polarization projections and $\tilde{S}_4 \equiv P$ the circular polarization. Thus $\underline{\tilde{S}}$ describes completely the photon polarization. If a photon of momentum $\vec{k}$ and polarization $\underline{\tilde{S}}$ suffers a Compton scatter, then the resultant Stokes vector is $\underline{S}' = \underline{\underline{T}}\,\underline{\underline{M}}\,\underline{\tilde{S}}$ and the resultant polarization is given by $\underline{\tilde{S}}' = \underline{S}'/I'$. The matrix $\underline{\underline{M}}$ rotates the linear polarization components between scatters since the coordinate system [12] for $\tilde{S}_3$ is defined by the scattering plane. $\underline{\underline{I}}$ itself is a function of $\vec{k}$, $\vec{k}'$ and $\vec{s}$. The Compton cross section is simply $\frac{d\sigma}{d\Omega} = I'$. In our calculation we assign every initial photon a Stoke's vector (1, 0, 0, 1). After each scatter we renormalize $\underline{S}'$ to $\underline{\tilde{S}}'$.

Several authors [45,46] in analyzing multiple scattering in transmission polarimeters have omitted the linear polarization components. This is incorrect since the geometry (source, magnet, detector) correlates successive scattering planes. Even though the initial photon lacks linear polarization,the first scatter will linearly polarize the photon and subsequent scatters will "analyze" it. This will affect both the detected intensity and the circular polarization efficiency. Despite cylindrical symmetry the correlations will <u>not</u> average out completely, however the resultant contribution from linear polarization effects is not expected to be very large.

Recall that every electron in the magnet is assigned a polarization of value f in the z-direction. In our system $f = \pm f_0$ where $f_0 = .067$. All quantities depending on f are expanded as polynominals, for example $\underline{S} = \underline{S}^{(0)} + \underline{S}^{(1)}\, f + \underline{S}^{(2)}\, f^2$, neglecting consistently terms beyond order f^2. Throughout the program only the coefficients themselves are evaluated while f is left as a free parameter. In

particular we carry a statistical "weight polynomial", initialized to unity at the source, along with each photon traced through the system. In the generation of random scattering positions and directions we use spin-independent cross sections as if f = 0. Then we adjust the weight polynomial to correct implicitly for the dependence on f. No bias is introduced by this procedure, moreover it is essential for an efficient Monte Carlo program. (The "simpler" techniques of running a program explicitly with $f = + f_0$ and then $f = -f_0$ (and f = 0 for information on quadratic terms) and comparing results to deduce the efficiency, would be far inferior statistically.)

As an example, suppose we have generated a scattering distance within the magnet $d = -\frac{1}{n\sigma_T} \ln r$ where n is the electron density, σ_T is the total spin-independent (f = 0) photon cross section per electron and r is a random number between 0 and 1. To allow for absorption we multiply the weight by $\frac{\sigma_0}{\sigma_T}$ where σ_0 is the Compton spin-independent cross section. To allow for f, the weight should be multiplied by the polynomial expansion of $e^{-f\tilde{S}_4(f)nd\,\sigma_c\cos\psi}(1 + f\,\tilde{S}_4(f)\,\frac{\sigma_c}{\sigma_0}\cos\psi)$, where σ_c is the spin dependent term of the Compton cross section [12] and ψ is the angle between $\vec{k}$ and $\vec{s}$.

The directions are generated by random sampling[47] of $S_1^{(0)'}$, since the probability distribution function for directions cannot be inverted analytically. The correction factor to the weight polynomial in this case is simply $1 + \frac{S_1^{(1)'}}{S_1^{(0)}} f + \frac{S_1^{(2)'}}{S_1^{(0)}} f^2$. For the forced scatters to the detector the zero-order probability is $S_1^{(0)'}\Delta\Omega e^{-nd_{OUT}\sigma_0}/\sigma_0$ where $\Delta\Omega$ is the solid angle of the unobscured part of the detector and d_{OUT}

is the path length out of the magnet. After a final adjustment here, the weight polynomial is added to the histogram discussed earlier. Then with reduced probability we proceed with multiple scatters from the last magnet point.

After tracing the desired number of initial photons with energy k_s we print out the terminal category information and the polynomial coefficients $N^{(n)}(k_D, z_M)$, meaning the $n^{\underline{th}}$ order term in f of the probability of detecting a photon with energy in bin k_D arising from magnet bin z_M. We then project the two-dimensional histogram $N^{(n)}(k_D, z_M)$ to obtain the following three one dimensional histograms: $N^{(n)}(k_D) = \sum_{z_M} N^{(n)}(k_D, z_M)$, $N^{(n)}(z_M) = \sum_{k_D} N^{(n)}(k_D, z_M)$ and $W^{(n)}(z_M) = \sum_{k_D} N^{(n)}(k_D, z_M) \cdot k_D/k_S$. The latter histogram (appropriate to our integral detection technique) is the expectation of <u>energy</u> detected relative to the initial energy. The final result for each energy k_s and given filter thickness w are the three numbers $D_n = D_n(k_s) = \sum_{z_M} W^{(n)}(z_M)$, for n = 0, 1 and 2.

In Fig. A.1(b) we show smoothed results for the intermediate histogram (bin size Δz_M = 1 cm) $W^{(0)}(z_M)$ (normalized to D_0) and the "efficiency" $-W^{(1)}(z_M)/W^{(0)}(z_M)$ for the representative initial energies k_s = 1 and 2 (in units of electron mass m). These indicate the relative effects of different parts of the magnet.

In Fig. A.1(c), we show the other smoothed projection $N^{(0)}(k_D)$ (bin size $\Delta k_D = k_s/10$) normalized to $N_0 \equiv \sum_{k_D} N^{(0)}$ and the corresponding efficiency $-N^{(1)}(k_D)/N^{(0)}(k_D)$. $N^{(0)}(k_D)$ is the detected spectrum for given initial energy k_s. We note that the efficiency peaks more

sharply for the higher energy curve $k_s = 2$, showing that the degradation from multiple scattering (the lower end of the spectrum) is more severe at higher k_s. We discuss this further below.

In Fig. A.2 we have plotted smoothed curves of $D_0(k_s)$, $-D_1(k_s)/D_0(k_s)$ and $D_2(k_s)/D_0(k_s)$ vs k_s/m. The error of each curve is about 5%. For each initial energy k_s and filter thickness w we had traced 1000 γ's from the source, resulting in roughly 2000 detected photons according to our branching technique. On the IBM 360/75 the average execution time was 25 ms per initial gamma. The values of $\frac{k_s}{m}$ used were 0.2, 0.4, ...,2.2, 2.4, 3,0, 3.5, 4.0 (note that pair production was not included in the program as we were actually concerned only with $\frac{k_s}{m} < 2$ in our experiments). We allowed no more than four random scatters each in the filter and the magnet, not counting the forced scatter. For comparison we ran once without the filter allowing zero random scatters in iron to see the differences between multiple scattering and "single scattering" calculations. The striking feature of the calculation is that for $k_s > m$ the multiple scattering efficiency factor D_1/D_0 saturates at -.33 whereas for single scattering alone it would continue to increase. This can be understood in part by inspection of the detected energy spectra for $k_s/m = 1, 2$ in Fig. A.1(c). We see that for higher k_s the efficiency falls off more rapidly away from the most probable k_D (mostly single scattered photons). Thus as k_s increases, multiple scatters through unfavorable angles (appearing in the low energy part of the k_D spectrum) dilute the efficiency more and more. The inadequacy of "single scattering" calculations is even more severe for the function D_2/D_0.

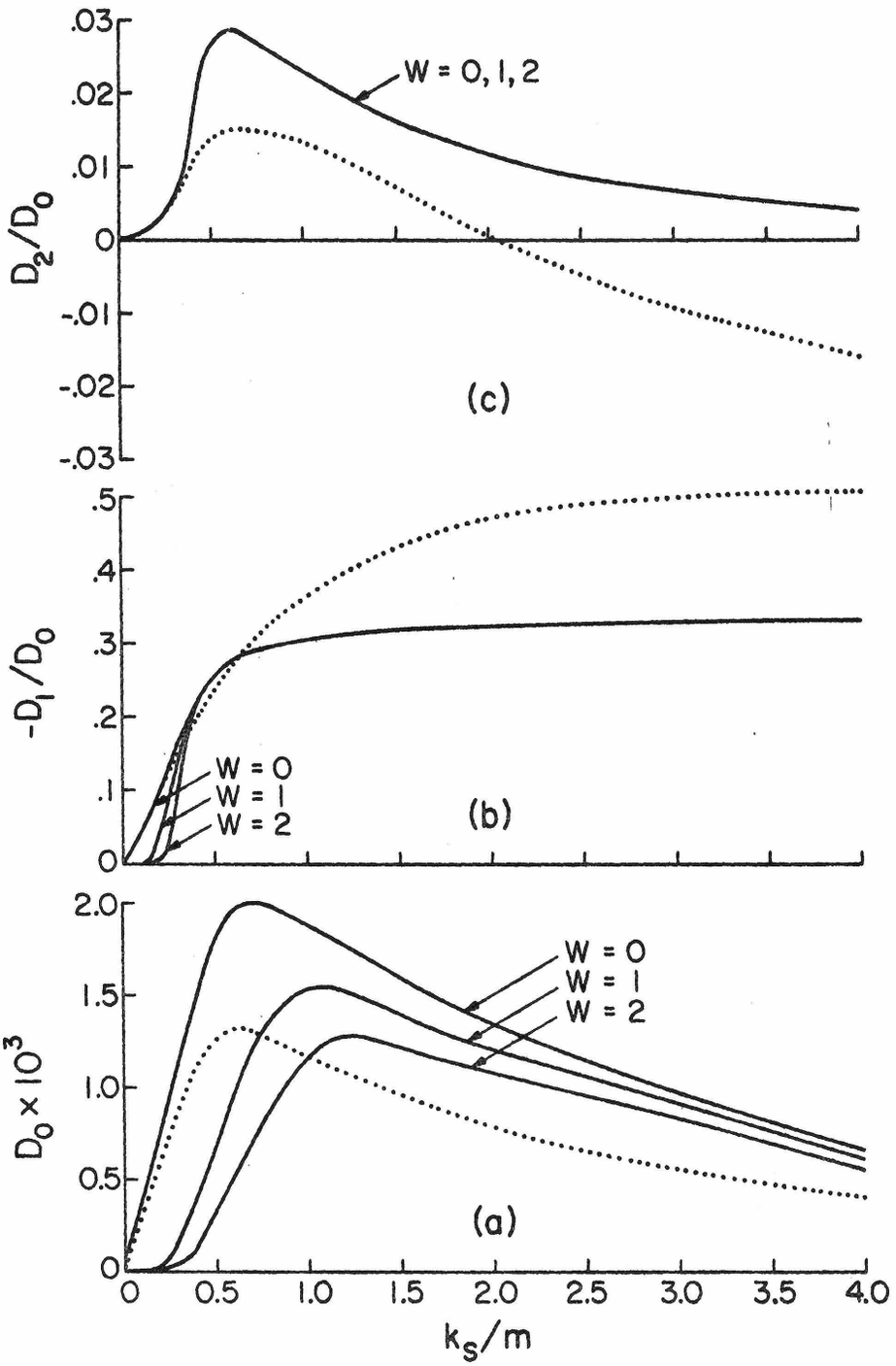

Fig. A.2 Smoothed results of Monte Carlo calculations; solid curves are multiple scattering results for lead filter thickness w = 0, 1, 2 and dotted curves are "single scattering" results for w = 0. (a) Intensity function D_0, (b) efficiency function $-D_1/D_0$, (c) quadratic function D_2/D_0.

The results thus testify to the importance of realistic multiple scattering calculations of the efficiency for such an integral detection (i.e. without energy resolution) Compton polarimeter.

A.3 Source Attenuation Function $A_s(k)$

In Section A.1 we introduced the function $A_s(k)$ for attenuation of photons in the source material and capsule wall (thickness ΔR_w). We have treated this problem as if each γ originated at a point on the axis of a cylinder of source material with radius $R_{EFF} = \frac{8}{3\pi} \times$ (actual source radius). We took a representative angle of 45° to the axis for the initial photon. Then (with the help of empirical formulas for the photoelectric absorption cross section τ_{PE} and the analytic Compton cross section σ_a for energy loss to electrons[48]) we computed for the density (ρ_i) of each element (Z_i, A_i) the mass absorption coefficient $\mu_{a,i}$. The resultant attenuation was given by

$$A_s(k) = \exp\left(-\left(\sum_{SOURCE} \mu_{a,i}\, R_{EFF}/\cos 45°\right)\right.$$

$$\left. - \left(\sum_{WALL} \mu_{a,i}\, \Delta R_w/\cos 45°\right)\right)$$

APPENDIX B

BREMSSTRAHLUNG CALCULATIONS

B.1 External Bremsstrahlung

Consider the emission of a β-particle of kinetic energy T' (velocity β') from a point within a material composed of one element Z; the latter restriction will be removed below. Assume that all β's are stopped within the material (i.e. range $\ll$ volume/surface). After numerous atomic collisions the electron will on the average have its energy reduced to T after having traveled a path length s and net displacement r. Suppose now that at r it interacts with the nuclear Coulomb field to produce "external bremsstrahlung" (EB). Averaging over the initial β direction and integrating over the volume of the material and the final direction Ω_k of the quantum, we obtain for the probability of producing a bremsstrahlung quantum with energy k to k + dk

$$dN_{k,T'} = \int_{\Omega_k} \int_{\Omega} \int_{r} \left(\frac{d^2\sigma_{BH}}{dk d\Omega_k} \, dk d\Omega \right) \left(\frac{1}{4\pi r^2} \right) \left(nr^2 dr d\Omega \right) \quad (B.1)$$

where n is the atomic density and $\frac{d^2\sigma_{BH}}{dk d\Omega_k}$ is the Bethe-Heitler bremsstrahlung cross section. This reduces to

$$\frac{dN_{k,T'}}{dk} = n \int_0^{\infty} dr \quad \frac{d\sigma_{BH}}{dk} \quad (B.2)$$

but since r is a measure of the electron energy

$$dr = -\frac{dT}{-\frac{dT}{dr}} = -\frac{dT}{\left(-\frac{dT}{ds}\right)\left(\frac{ds}{dr}\right)} \tag{B.3}$$

therefore

$$\frac{dN_{k,T'}}{dk} = \int_0^{T'} dT \; \frac{\frac{d\sigma_{BH}}{dk}}{\left(-\frac{1}{n}\frac{dT}{ds}\right)\left(\frac{ds}{dr}\right)}$$

which agrees with eqn.(43) of Ref.(49)for "fast" electrons, except for our refined factor $\frac{ds}{dr}$.

At this point we introduce the β spectrum $\frac{dN_\beta}{dT'}$ normalized such that

$$\int_0^{T_m} dT' \; \frac{dN_\beta}{dT'} = 1$$

where T_m is the endpoint. Then the EB probability density is

$$\frac{dN_{EB}}{dk} = \int_0^{T_m} dT' \; \frac{dN_\beta}{dT'} \; \frac{dN_{k,T'}}{dk} \tag{B.4}.$$

Whereas $\frac{d\sigma_{BH}}{dk}$ and $-\frac{dT}{ds}$ are well known analytically, the general dependence of $\frac{ds}{dr}$ on T and Z is unknown; Evans[50] indicates that it is generally in the range of 1.2 to 4.9. However we note that the variation of $\frac{ds}{dr}$ with T and Z is very gradual compared with that of $\frac{d\sigma_{BH}}{dk}$ and $\frac{dT}{ds}$. Therefore we remove $\frac{ds}{dr}$ from the integral in an average sense defined by

$$\frac{dN_{EB}}{dk} = \frac{1}{\zeta}\int_0^{T_m} dT' \; \frac{dN_\beta}{dT'} \int_0^{T'} dT \; \frac{\frac{d\sigma_{BH}}{dk}}{-\frac{1}{n}\cdot\frac{dT}{ds}} \tag{B.5}$$

where we have introduced a "zigzag parameter" $\zeta = \left\langle \frac{ds}{dr} \right\rangle$. We have determined experimentally (see Sec. III. 3(b)) that $\zeta \approx 1.5$ for our cases.

For the circular polarization P(k) we obtain similarly

$$P(k)\,\frac{dN_{EB}}{dk} = \frac{1}{\zeta}\int_0^{T_m} dT' \; \frac{dN_\beta}{dT'} \int_0^{T'} dT \; \frac{\frac{d\sigma_c}{dk}}{-\frac{1}{n}\frac{dT}{ds}} \tag{B.6}$$

where $\frac{d\sigma_c}{dk}$ is the polarization dependent component of the bremsstrahlung cross section.

The generalization of the integrands of equations (B.5), (B.6) to homogenous material with several elements Z_i with atomic weight A_i and (relative) masses M_i is

$$\frac{\frac{d\sigma}{dk}}{-\frac{1}{n}\frac{dT}{ds}} \rightarrow \frac{\sum_i \frac{M_i}{A_i}\left[\frac{d\sigma}{dk}\right]_{Z_i}}{\sum_i \frac{M_i}{A_i}\left[-\frac{1}{n}\frac{dT}{ds}\right]_{Z_i}} \tag{B.7}.$$

Now, $\frac{d\sigma_{BH}}{dk}$ and $\frac{d\sigma_c}{dk}$ are essentially proportional to Z^2 except for a small screening correction and $\frac{1}{n}\frac{dT}{ds}$ is essentially proportional to Z except for the logarithmic Z dependence through the excitation potential. Thus with fair accuracy (25%) we could evaluate the EB for

a uniform source with effective Z

$$Z_{eff} = \frac{\Sigma \frac{M_i}{A_i} Z_i^2}{\Sigma \frac{M_i}{A_i} Z_i} \qquad (B.8).$$

Note moreover that the EB intensity is in our approximation directly proportional to Z_{eff}. We have listed the values of Z_{eff} for each source in Table III.2. In actual computations we used the more accurate formula (B.7).

For the normalized β-spectrum we have used the formula

$$\frac{dN_\beta}{dT'} = 30 \frac{(T' + 1)^2 (T_m - T')^2}{T_m^3 (T_m^2 + 5T_m + 10)} \qquad (B.9)$$

which assumes a Fermi function $F(Z,W') \propto W'/p' = 1/\beta'$, which is quite good for our β-decays which are all allowed or first parity forbidden and have $T_m < 1$ MeV.

For the electron energy loss, neglecting bremsstrahlung, we have used [51]

$$-\frac{1}{n}\frac{dT}{ds} = \frac{2\pi Ze^2}{\beta^2}\left[\ln \frac{\beta^2 (T + 1)}{2I^2 (1 - \beta^2)} - (2 (1 - \beta^2)^{1/2} - 1 + \beta^2) \ln 2 + 1 - \beta^2 + \frac{1}{8}(1 - (1 - \beta^2)^{1/2})^2\right] \qquad (B.10)$$

where β is the electron velocity and I is the atomic excitation potential; we used[52] $I = \frac{9.3\ Z}{.511 \times 10^6}$ for $Z > 15$ (actually $Z \geq 44$ in our cases) and $I = \frac{12.7\ Z}{.511 \times 10^6}$ for $Z \leq 15$, viz. C and O.

For bremsstrahlung we used the involved formulas of Fronsdal and Überall[53] for $\frac{d\sigma_{BH}}{dk\ d\ \cos\theta}$ and $\frac{d\sigma_c}{dk\ d\ \cos\theta}$, including atomic screening effects. In the evaluation of $\frac{d\sigma_c}{dk}$ we took the electron longitudinal polarization to be $-\beta'$, thereby neglecting depolarizing effects of collisions. The cross sections are calculated in the Born approximation $\frac{Z}{137\beta} \ll 1$, which, may lead to an underestimate[54] by a few percent in our energy range. This in turn would induce a corresponding underestimate of $\left\langle \frac{ds}{dr} \right\rangle$ when we determine ζ by comparing theory and experiment. In other words ζ is not solely a parameter for path lengths but also incorporates a correction (perhaps negligible) to the Born approximation.

B.2 Internal Bremsstrahlung

During β-decay the electron interacts with the Coulomb field of the daughter nucleus producing "internal bremsstrahlung" (IB), which is circularly polarized. The spectrum of IB is given[55] approximately by

$$\frac{dN_{IB}}{dk} = \int_{1+k}^{W_0} dW_e \ \frac{dN_\beta}{dW_e} \ \Phi(W_e,\ k) \qquad (B.11)$$

$$\Phi(W_e,k) = \frac{p}{137\pi\ p_e k} \left[\frac{W_e^2 + W^2}{W_e p} \cdot \ln\ (W + p) \ -2 \right] \qquad (B.12)$$

where $W_e = (T_e + 1)$ and p_e are the total energy and momentum of the (virtual) electron before emission of an IB quantum of energy k and

$W = (T + 1)$ and p are the energy and momentum of the final state electron; thus $W_e = W - k$.

For the normalized β- spectrum $\frac{dN_\beta}{dW_e}$ (or $\frac{dN_\beta}{dT_e}$) we have used a form similar to (B.9), except that the Fermi function now applies to the final state electron viz $F(Z,W) \alpha W/p$:

$$\frac{dN_\beta}{dW_e} = 30 \frac{(T_e + 1)^2 (T_m - T_e)^2}{T_m^3 (T_m^2 + 5 T_m + 10)} \cdot \frac{p_e W}{W_e p} \qquad (B.13)$$

where the normalization is no longer exact; however since the IB peaks sharply at $k = 0$ ($W_e = W$, $p_e = p$), the normalization error is very minor.

The polarization is given by

$$P(k) = - \frac{J_2(k)}{J_1(k) + J_2(k)} \qquad (B.14)$$

where the analytic functions $J_1(k)$ and $J_2(k)$ are given by Pytte[56].

B.3 Results of Calculations

In Fig.B.1(a) we show typical results for IB and EB polarization and energy spectra $k\frac{dN}{dk}$ for the 962 keV β-decay of Au_2O_3 diluted and undiluted and in Fig.B.1(b) for the 497 keV β-decay of Lu^{177} diluted only. Note that photon attenuation in the source material is not included in these spectra (see Appendix A). The calculated EB spectra shown do not include the correction factor $1/\zeta$.

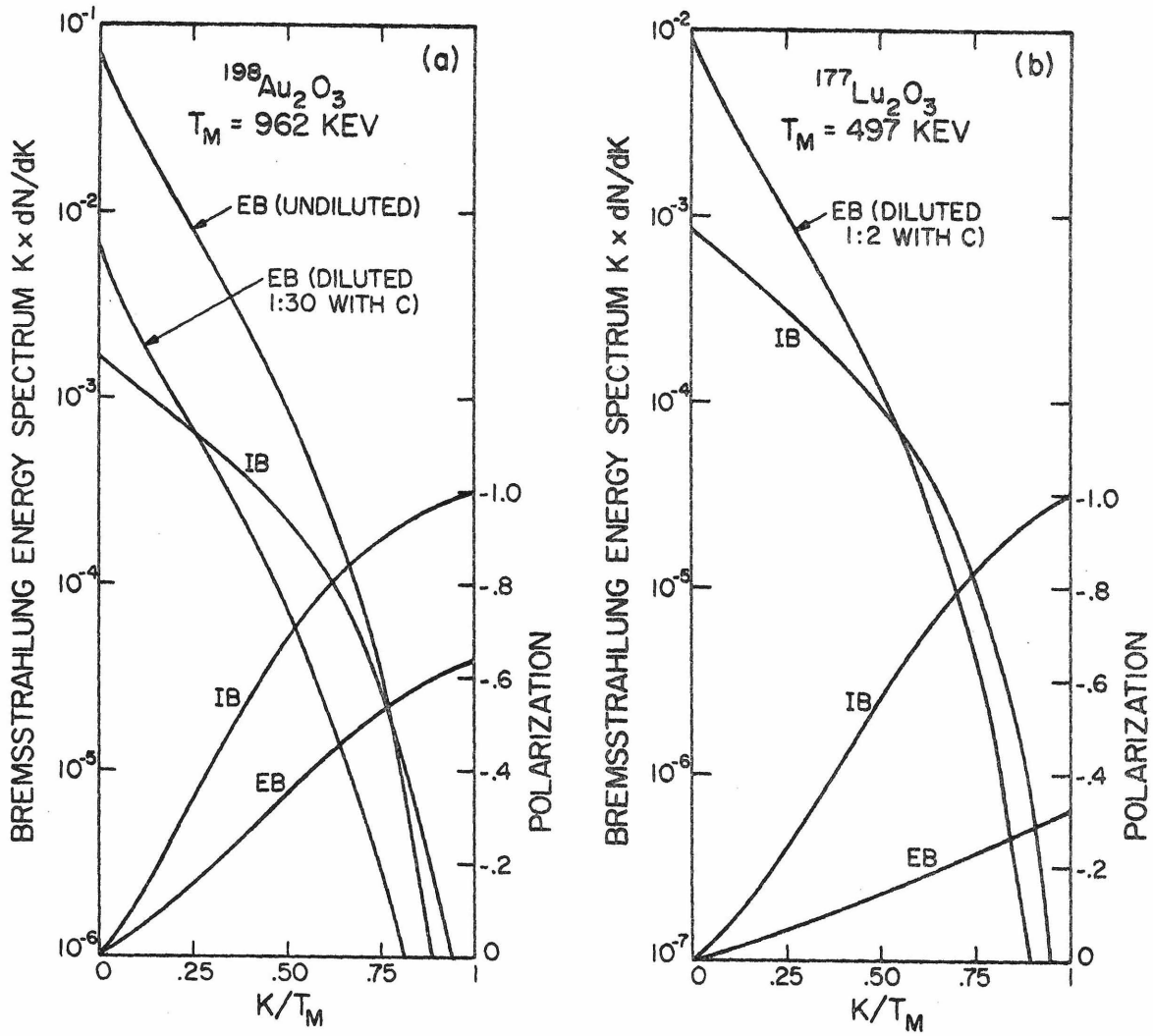

Fig. B.1 Internal (IB) and external (EB) bremsstrahlung energy spectra and polarization. The correction factor $1/\zeta$ is not included in the EB spectra. (a) ^{198}Au 962 keV β decay, (b) ^{177}Lu 497 keV β decay.

APPENDIX C

EFFECTS OF THE QUADRATIC TERM D_2 (k)

In Appendix A, we have shown that the detector current I has some non-linear dependence on f, the fraction of polarized electrons, arising from absorption and multiple scattering processes. In a polynomial expansion of I, the odd terms (in particular the linear term) in f are proportional to the initial γ circular polarization P, while the even terms (in particular the quadratic term) are independent of P. Thus if the magnetization is unequal in the two states we will observe an asymmetry even if P = 0. This is both a disadvantage in that it requires precise symmetry in the magnet current I^M in order to avoid "false" asymmetries and an advantage in that it offers an alternative technique for calibrating the system with an unpolarized beam of monochromatic γ-rays (as opposed to the continuous spectrum of polarized bremsstrahlung). For discussions of an analogous technique for calibrating transmission polarimeters see references (57) and (58).

For simplicity then consider a source of monochromatic photons of energy k with zero net circular polarization. Then from Appendix A we have

$$I(t) = I_0 + I_2(t) \tag{C.1}$$

with

$$I_0 = CkD_0(k) \tag{C.2}$$

$$I_2(t) = f(t)^2\, Ck\, D_2(k) \tag{C.3}$$

where C is a constant. As discussed in Sec. A.1, we neglect terms $O(f^3)$.

Let

$$Q(k) = D_2(k)/D_0(k) \tag{C.4}$$

and

$$Q^*(k) = f_0^2\, Q(k) \tag{C.5}.$$

Then

$$I = I_0\ (1 + Q(k)f^2) \tag{C.6}$$

or

$$I = I_0\ (1 + Q^*(k)\ (f/f_0)^2) \tag{C.7}.$$

If $f(t)$ is a perfect square wave then $f(t)^2$ is essentially a constant and the only effect is a negligible renormalization to I_0. More generally consider a function $f(t)$ (Fig. C.1) which is a trapezoidal distortion of a square wave (linear reversal in time interval T_s) with an amplitude asymmetry $\delta = \frac{f_1 - f_2}{f_1 + f_2}$, with a timing asymmetry $\epsilon = \frac{t_1 - t_2}{t_1 + t_2}$ and with a phase shift $\alpha\pi$ with respect to the LIA mixer (synchronous rectifier) waveform $r(t)$, which itself has a timing asymmetry γ; in addition allow an asymmetry ρ in the areas of the resultant quadratic pulses of $f(t)$, due for example to unequal reversal times. If all these distortions are small then the resultant asymmetry will be linear in each. If α, ϵ, γ and ρ are all zero, then for small δ we obtain

$$A_{AMPL} = \frac{I_1 - I_2}{I_1 + I_2} = 2Q^*\delta \tag{C.8}.$$

The maximal effect occurring with $f_1 = f_0$, $f_2 = 0$ is

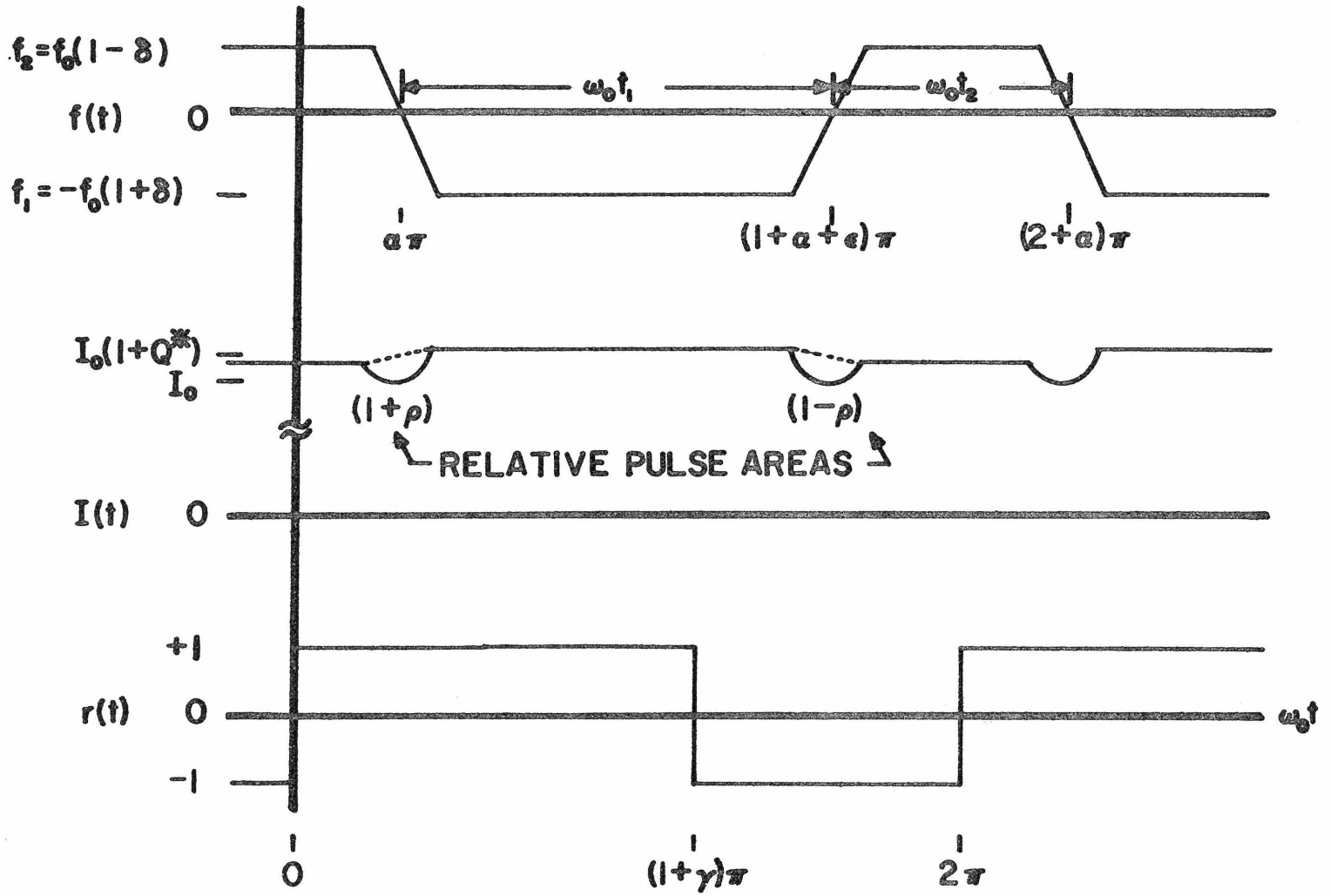

Fig. C.1 Waveform distortions leading to asymmetries via the term in I(t) which is quadratic in f(t). See text.

$$A_{ON-OFF} = Q^*/2 \qquad (C.9)$$

The quadratic pulses that appear in I(t) ideally contribute only to even harmonics of ω_0 and are thereby rejected. However in the presence of the timing distortions, we find (in the case $\delta = 0$) after a lengthy Fourier analysis the approximate result

$$A_{TIME} \approx \frac{\pi}{6} \omega_0 T_S Q^*[\epsilon + (2\alpha - \gamma)\rho] \qquad (C.10)$$

We have measured Q^* for the 497 keV γ-ray of ^{103}Ru using (C.9) and (C.10). In the former case we fixed I_1^M at its normal saturation value so that $f_1 = f_0$; then the value of I_2^M yielding $f_2 = 0$ was determined implicitly by scanning I_2^M through small negative values seeking the maximum A_{ON-OFF}. This gave

$$Q^* = (1.24 \pm 0.02) \times 10^{-4} .$$

In the latter case we measured A_{TIME} vs ϵ and deduced

$$Q^* = (0.9 \pm 0.2) \times 10^{-4} .$$

The Monte Carlo evaluation of Q at this energy (Fig. A.2(c)) is

$$Q = 0.023 \pm 0.002.$$

With our value $f_0 = .067$ we would estimate

$$Q^* = 1.03 \pm 0.10$$

in reasonable agreement with the experimental values above.

Finally as a function of small current amplitude asymmetry $\eta = \dfrac{I_1^M - I_2^M}{I_1^M + I_2^M}$ we have measured $A_{AMPL}/\eta = (1.8 \pm 1.6) \times 10^{-6}$ and

determined using Eqn. (A3-8) and our measured Q^* that at saturation on our dynamic hysteresis loop, $\frac{dB/B}{dH/H} = \frac{\delta}{\eta} = .075 \pm .007$.

If we had not known f_0 for our material we could in fact have deduced it by comparing the Monte Carlo calculation of Q with measurements of Q^*. An alternative way is comparing bremsstrahlung polarization calculations with experimental asymmetries but this requires complicated and somewhat uncertain calculations of bremsstrahlung spectra and polarization. Thus we offer these techniques with the quadratic term as a simple but valuable tool in studying the properties of forward scattering polarimeters.

Now we turn to the problem of suppressing these quadratic terms in parity measurements. For this purpose it is important to know Q and Q^*. On our "magnet control" circuits (Fig. II.3), we included adjustments for δ and ϵ; the lock-in amplifier has adjustments for α and γ; the zener diodes in the power amplifier feedback determine ρ. Measurements gave the following limits: for timing $|\epsilon| < 0.001$, $|\alpha| < 0.02$, $|\gamma| < 0.02$, $|\rho| < 0.005$, and for amplitude $|\eta| < 0.001$ and so $|\delta| < 7.5 \times 10^{-4}$. Thus in parity experiments $|A_{TIME}| < 3 \times 10^{-8}$ and $|A_{AMPL}| < 2 \times 10^{-8}$. Such residual asymmetries are corrected for by means of control experiments.

REFERENCES

1. T.D. Lee and C.N. Yang, Phys. Rev. 104, 254 (1956).
2. For a review of β-decay parity experiments see:C.S. Wu, Revs. Mod. Phys. 31, 783 (1959).
3. R.P. Feynman and M. Gell-Mann, Phys. Rev. 109, 193 (1958).
4. H. Schopper, Nucl. Inst. 3, 158 (1958).
5. V.M. Lobashov, V.A. Nazarenko, L.F. Saenko, L.M. Smotritsky and G.I. Kharkevitch, Phys. Lett. 25B, 104 (1967).
6. J.C. Vanderleeden and F. Boehm, Phys. Rev. C2, 748 (1970).
7. E.M. Henley, Ann. Rev. Nucl. Sci. 19, 367 (1969).
8. R.J. Blin-Stoyle, Proc. Top. Conf. Weak Int., CERN, Geneva 495 (1969).
9. F. Boehm, Proc. Int. Conf. Ang. Correl. in Nucl. Disint., Delft (1970).
10. N. Cabibbo, Phys. Rev. Lett. 10, 531 (1963).
11. R.J. Blin-Stoyle, Phys. Rev. 120, 181 (1960).
12. H.A. Tolhoek, Revs. Mod. Phys. 28, 277 (1956).
13. Silectron ™ cores from Arnold Engineering Company, Fullerton, California.
14. Netic ™ and Co-netic ™ Foils, Magnetic Shield Division, Perfection Mica Company, Chicago, Illinois.
15. Model HR-8 Lock-in Amplifier, Princeton Applied Research Corporation, Princeton, New Jersey.
16. Model DF-115R Bipolar DC-to-Frequency Converter, Anadex Instruments Inc., Van Nuys, California.

17. Titanium alloy: 6% Al, 4% V, 0.2% Fe.

18. J.D. Bowman and J.C. Vanderleeden, Nucl. Instr. and Meth. 85 19, (1970).

19. P. Bock, Phys. Lett. 30B, 628 (1969).

20. P. Bock, Lett. Nuovo Cimento, 1, 157 (1971).

21. F. Brailsford and R.G. Martindale, J. Inst. Elec. Engrs. 89 ,225 (1942).

22. B. Jenschke and P. Bock, Phys. Lett. 31B, 65 (1970).

23. J.C. Vanderleeden, F. Boehm and E.D. Lipson, to be published.

24. F. Boehm and E. Kankeleit, Nucl. Phys. A109, 457 (1968).

25. E. Kankeleit and E. Kuphal, private communication.

26. P. De Saintignon and M. Chabre, Phys. Lett. 33B, 463 (1970).

27. P. Bock and B. Jenschke, Nucl. Phys. A160, 550 (1971).

28. J.J. van Rooijen, P. Pronk, S.U. Ottevangers and J. Block, Physica 37, 32 (1967).

29. D.W. Cruse and W.D. Hamilton, Nucl. Phys. 125, 241 (1969).

30. P. De Saintignon, J.J. Lucas, J.B. Viano, M. Chabre and P. Depommier, Nucl. Phys. A160, 53 (1971).

31. E. Bodenstedt, L. Ley, H.O. Schlenz and U. Wehman, Phys. Lett. 29B, 165 (1969).

32. P. Vogel, Internal Report CALT-63-155, Calif. Inst. of Tech. (1971).

33. P. Bock, B. Jenschke and H. Schopper, Phys. Lett. 22, 316 (1966).

34. R. Hager and E. Seltzer, Phys. Lett. 20, 180 (1966).

35. W.P. Pratt, Jr., R.J. Schermer, J.R. Sites, and W.A. Steyert, Phys. Rev. C2, 1499 (1970).

36. Z. Szymanski, Nucl. Phys. 76, 539 (1966).

37. F.C. Michel, Phys. Rev. 133, B329 (1964).

38. S. Wahlborn, Phys. Rev. 138,B530 (1965).

39. E. Maqueda and R.J. Blin-Stoyle, Nucl. Phys. A91, 460 (1967).

40. B.H.J. McKellar, Phys. Rev. Lett. 20, 1542 (1968).

41. N. Vinh Mau and A.M. Bruneau, Phys. Lett. 29B, 408 (1969).

42. M. Gari, O. Dumitrescu, J.G. Zabolitzky and H. Kümmel, Phys. Lett., to be published, 1971.

43. W.H. McMaster, Revs. Mod. Phys. 33, 8 (1961).

44. U. Fano, Revs. Mod. Phys. 29, 74 (1957).

45. R.B. Chesler, Nucl. Instr. and Meth. 37, 185 (1965) .

46. R.D.L. Mackie and J. Byrne, Nucl. Instr. and Meth. 74, 268 (1969).

47. E.D. Cashwell and C.J. Everett, A Practical Manual on the Monte Carlo Method for Random Walk Problems (Pergammon Press, New York, 1959) p. 9.

48. Nat. Stand. Ref. Data Ser.,Nat. Bur. Stand. (U.S.) 29 (1969) p. 24 ff.

49. H.A. Bethe and W. Heitler, Proc. Roy. Soc. (London) A146, 83 (1934).

50. R.D. Evans, The Atomic Nucleus (Mc Graw Hill, Inc., New York, 1955) p. 611.

51. H.A. Bethe and J. Ashkin in Experimental Nuclear Physics, Volume 1, E. Segrè, ed. (John Wiley and Sons, Inc., New York, 1953) p.254.

52. G. Knop and W. Paul in Alpha- Beta- and Gamma-Ray Spectroscopy, Vol. 1, K. Siegbahn, ed. (North-Holland Publishing Company, Amsterdam, 1966) p.13.

53. C. Fronsdal and H. Überall, Phys. Rev. 111, 580 (1958).

54. H.W. Koch and J. Motz, Revs. Mod. Phys. 31, 920 (1959).

55. J.K. Knipp and G.E. Uhlenbeck, Physica 3, 425 (1936).

56. A. Pytte, Phys. Rev. 107, 1681 (1957).

57. S.B. Gunst and L.A. Page, Phys. Rev. 92, (1953) 970.

58. R.D.L. Mackie and J. Byrne, Nucl. Instr. and Meth. 76, 241 (1969).